



**HAL**  
open science

## **Interactions between flow structure and morphodynamic of bars in a channel expansion/contraction, Loire River, France**

Nicolas Claude, Stéphane Rodrigues, Vincent Bustillo, Jean-Gabriel Bréhéret, Pablo Tassi, Philippe Jugé

► **To cite this version:**

Nicolas Claude, Stéphane Rodrigues, Vincent Bustillo, Jean-Gabriel Bréhéret, Pablo Tassi, et al.. Interactions between flow structure and morphodynamic of bars in a channel expansion/contraction, Loire River, France. *Water Resources Research*, 2014, 50 (4), pp.2850 - 2873. 10.1002/2013WR015182 . hal-01710051

**HAL Id: hal-01710051**

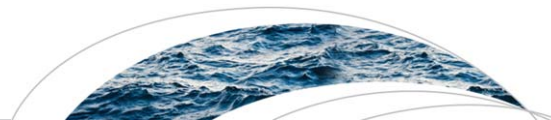
**<https://hal.science/hal-01710051>**

Submitted on 12 Nov 2021

**HAL** is a multi-disciplinary open access archive for the deposit and dissemination of scientific research documents, whether they are published or not. The documents may come from teaching and research institutions in France or abroad, or from public or private research centers.

L'archive ouverte pluridisciplinaire **HAL**, est destinée au dépôt et à la diffusion de documents scientifiques de niveau recherche, publiés ou non, émanant des établissements d'enseignement et de recherche français ou étrangers, des laboratoires publics ou privés.

Copyright



## RESEARCH ARTICLE

10.1002/2013WR015182

# Interactions between flow structure and morphodynamic of bars in a channel expansion/contraction, Loire River, France

Nicolas Claude<sup>1,2,3</sup>, Stéphane Rodrigues<sup>1</sup>, Vincent Bustillo<sup>4</sup>, Jean-Gabriel Bréhéret<sup>1</sup>, Pablo Tassi<sup>2</sup>, and Philippe Jugé<sup>5</sup>

### Key Points:

- Field measurements of flow around bars in a channel expansion/contraction
- Bars modify flow structure imposed by channel width variations
- Flow structure defined by planform and bars affects in turn bars morphodynamic

<sup>1</sup>Département Géosciences-Environnement, Université François Rabelais, Tours, France, <sup>2</sup>Laboratoire Saint-Venant, Université Paris-Est, Ecole Nationale des Ponts et Chaussées, EDF R&D, CETMEF, Chatou, France, <sup>3</sup>Ecole Nationale des Ponts et Chaussées, Marne-la-Vallée, France, <sup>4</sup>CESBIO UMR CNRS-IRD-CNES-UPS 5126, IUT Paul Sabatier, Auch, France, <sup>5</sup>CETU Elmis, Université François Rabelais, Chinon, France

### Correspondence to:

N. Claude,  
nicolas\_claude2000@yahoo.fr

### Citation:

Claude, N., S. Rodrigues, V. Bustillo, J.-G. Bréhéret, P. Tassi, and P. Jugé (2014), Interactions between flow structure and morphodynamic of bars in a channel expansion/contraction, Loire River, France, *Water Resour. Res.*, 50, 2850–2873, doi:10.1002/2013WR015182.

Received 16 DEC 2013

Accepted 26 FEB 2014

Accepted article online 3 MAR 2014

Published online 2 APR 2014

**Abstract** The study of the relationship between flow structure and morphodynamic of bars in a channel expansion/contraction is essential to better understand the processes that control the evolution of rivers. Thus, multibeam echosoundings and Acoustic Doppler Profiler (ADP) measurements were performed with a high temporal resolution in an expansion/contraction zone of the Loire River (France) occupied by bars. During the monitoring period, the macroforms presented successively an alternate, a lateral and a transverse configuration. Field data were analyzed to study how the primary and secondary velocities, the flow directions, the bed shear stresses, and the bed roughnesses (associated to dunes) evolve as a function of the water discharge and bars configuration. The bars modify the flow structure imposed by the channel width variations. In fact, the bars induce a topographic forcing which enables the separation and reducing of the mixing of two currents formed in the upstream channel expansion. This forcing is enhanced by the turbulence formed by the large dunes superimposed on the bars. Therefore, the bars promote a nonuniform flow in the channel. In turn, in the channel expansion/contraction, the migrating bars' morphodynamics are affected by the downstream channel narrowing which stops their downstream migration and forced the bars in the system. Then the nonuniformity of the flow encourages the lateral migration of the macroforms until they reach a bank and become nonmigrating. Finally, the nonmigrating bars are eroded by the flow deflected during the migration of a new bar in the channel expansion/contraction.

## 1. Introduction

Alluvial bars or macroforms are present in the majority of sandy and gravel rivers. The height and width of these bed forms are of the same order of magnitude as the water depth and the river width, respectively [Jackson, 1975]. The bars interact with the flows and sediment transport, and they exert a strong influence on the morphological evolution of rivers [Parker, 1976; Fredsoe, 1978; Blondeaux and Seminara, 1985; Struiksmas et al., 1985; Crosato and Mosselman, 2009; Kleinhans and van den Berg, 2011].

There are two different types of bars: free bars and forced bars [Seminara and Tubino, 1989]. Free bars (migrating or not) are created by the instability of turbulent flows over an erodible bed [Callander, 1969; Colombini et al., 1987; Seminara and Tubino, 1989; Tubino, 1991]. Studies regarding free bars are generally numerical [Defina, 2003; Bernini et al., 2006] experimental [Lisle et al., 1991; Tubino, 1991; Lanzoni, 2000a, 2000b], or both [Crosato et al., 2011, 2012] and concern essentially their formation. In contrast, field studies are rare [Leopold and Wolman, 1957; Lewin, 1976; Rodrigues et al., 2012], and the morphology of these bars in natural rivers and their influence on the structure of flow and sediment transport have not been well studied [Whiting and Dietrich, 1991].

Forced bars are quasi-stationary structures that develop under the influence of planimetric constraints such as curvature and width variations of a channel. The effect of curvature usually leads to the formation of point bars [Ikeda and Parker, 1989] which in turn, have an effect on the flow structure and sediment transport [Bridge and Jarvis, 1982; Dietrich and Smith, 1983, 1984]. Forced bars that are associated with the convergence and divergence of flow in a channel expansion/contraction appear as midchannel bars or as two symmetrical lateral bars [Bittner, 1994; Repetto et al., 2002; Wu and Yeh, 2005; Luchi et al., 2010a, 2010b; Wu et al., 2011]. Interactions between hydro-sedimentary processes and bed morphology around midchannel

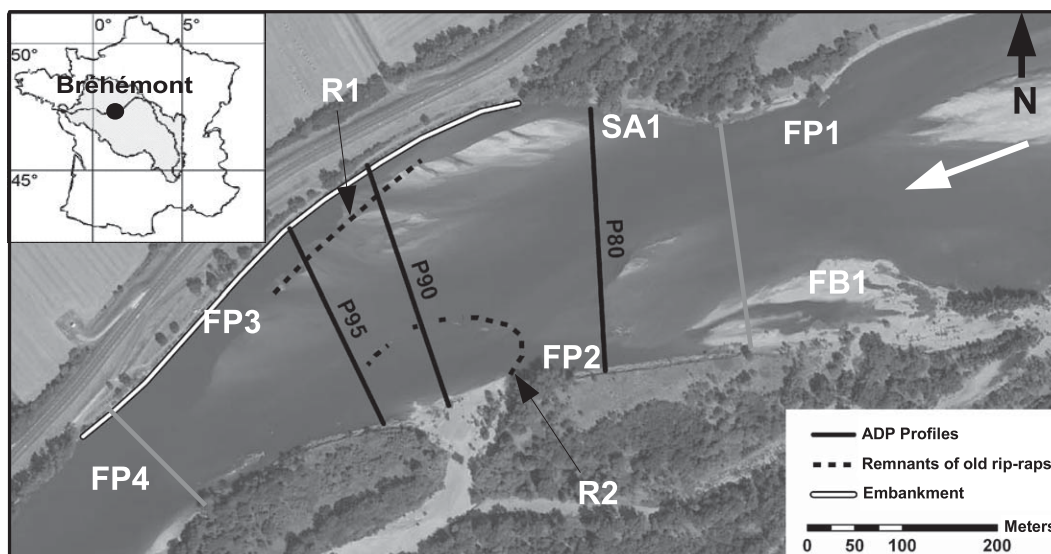


**Figure 1.** Presentation of the study site. The gray lines denote the upstream and downstream limits of the expansion/contraction zone. The white arrow denotes the flow direction. See text for an explanation of additional labels.

bars have been the subject of numerous field investigations [Leopold and Wolman, 1957; Whiting and Dietrich, 1991; Ashworth *et al.*, 1992; Bridge and Gabel, 1992; Ferguson *et al.*, 1992; Richardson *et al.*, 1996; Richardson and Thorne, 1998, 2001; McLelland *et al.*, 1999] and experimental studies [Ashmore, 1982, 1991; Ashworth, 1996; Federici and Paola, 2003]. In contrast, the structure of flow and sediment transport has been seldom studied when lateral bars occupy channel widening. Recently, Wu *et al.* [2011] highlighted that the migration of free bars (in alternate configuration) on forced bars (transverse bars or lateral bars) in a channel of variable width could give rise to mixed bars (free + forced). These mixed bars are arranged in alternate or transverse configurations according to the migration of the free bars. However, the evolution of flow structure as a function of different bar configurations is not described in this study.

There remains a lack of data concerning the flow structure around alternate bars in a natural setting, particularly when they occupy a channel widening. Furthermore, the relationship between the hydrodynamic and morphodynamic of macroforms in a channel expansion/contraction (without changing the planform) successively occupied by alternate bars and transverse bars has not been documented.

Accordingly, hydraulic and bathymetric data were acquired from the middle reach of the Loire River (France). In this relatively large sandy-gravel river, sediments are mobile [Rodrigues and Claude, 2010], and significant morphological changes were observed even during periods of low or medium flow [Claude, 2012]. The combination of continuous sediment transport and the forcing effects caused by channel width variations [Wu *et al.*, 2011] can induce the succession of alternate or transverse bars at certain channel expansion/contraction of the Loire River. First, this study, based on the analysis of flow measurements and bathymetric data describes the influence of alternate and transverse bars on flow structure in a channel expansion/contraction, with fixed banks, for different water discharges. Second, the feedbacks of flows on bar morphodynamics are discussed in order to highlight the processes allowing the succession of the different bars configurations in the studied reach.

## 2. Loire River and Study Site

### 2.1. Presentation of the Loire River

The Loire River, the largest river in France, is 1020 km long and drains a catchment area of 117,000 km<sup>2</sup>. The study site (Figure 1) is located 790 km downstream from the source, near the village of Bréhémont (47°17'43.31"N, 0°20'33.80"E) in the middle reach of the Loire River. At the study site, the Loire system presents an incised multiple-channel pattern composed of a braided main channel, vegetated permanent

islands, and secondary channels that are only submerged during floods [Rodrigues *et al.*, 2006; Détriché *et al.*, 2010]. The incision of the main channel has caused many problems including the destabilization of civil engineering works, the decrease of the flow capacity during floods, the lowering of the water table, and the development of the pioneer vegetation in the secondary channels [Bravard *et al.*, 1997; Belleudy, 2000; Rodrigues *et al.*, 2007].

## 2.2. Study Site and Channel Morphology

At the Langeais gauging station (4.5 km upstream of the study site), the water discharge has an annual average of  $430 \text{ m}^3 \text{ s}^{-1}$  and is  $\sim 1900 \text{ m}^3 \text{ s}^{-1}$  during a 2 year flood. The studied main channel is composed of an expansion zone followed by a contraction area (Figure 1) occupied by bars. The width of the main channel varies between 175 and 300 m. The right bank is protected by rip-raps on the downstream part of the study site (Figure 1). The bed load is mainly composed of siliceous sand and gravel. The  $D_{50}$  and  $D_{90}$  (diameters for which 50 and 90% of the particles in weight are finer, respectively) of the bed sediments are 1.33 and 5.18 mm, respectively.

Several stable morphological units are located in the main channel. Upstream the expansion area, a forced bar (FB1) is found near the left bank just downstream of a small island and a forced pool (FP1) at the foot of the right bank (Figure 1). A stagnation area (SA1) is located near the right bank in the expansion area. Two forced pools are also present: the first (FP2) at the foot of the left bank near profile P80, the second (FP3) at the foot of the rip-rapped section of the right bank (Figure 1). The profiles, P80, P90, and P95, monitored during flow measurements are 277, 265, and 230 m wide, respectively. On these cross sections, the aspect ratio, defined by  $W/d$  (where  $W$  is the channel width and  $d$  is the average water depth) decreases from upstream to downstream and change with the water discharge. For example, on P80, the aspect ratio reaches 56 at  $1950 \text{ m}^3 \text{ s}^{-1}$  and 159 at  $386 \text{ m}^3 \text{ s}^{-1}$  (Figure 2). Moreover, on the same cross section, for the water discharges considering in this study, the mean flow velocities vary between  $0.79$  and  $1.31 \text{ m s}^{-1}$  and the water depth between 1.73 and 4.93 m (Figure 2). The average slope of the main channel fluctuates around  $30 \text{ cm km}^{-1}$  in this area.

Finally, stretches of rip-rap, vestiges of ancient bank protections, are located in the channel near the right bank between P90 and P95 (R1 on Figure 1) and face the entrance of a secondary channel (R2 on Figure 1). The connection of this channel starts at  $700 \text{ m}^3 \text{ s}^{-1}$  but the inlet step of the channel is totally submerged only above  $1700 \text{ m}^3 \text{ s}^{-1}$ .

## 3. Materials and Methods

The work presented in this paper is based on bathymetric data obtained with a multibeam echosounder and flow measurements taken from an Acoustic Doppler Profiler (ADP). The data were collected between March 2010 and January 2011 (Figure 3). Three floods were particularly detailed: one annual freshet in June with discharges varying between  $386$  and  $1030 \text{ m}^3 \text{ s}^{-1}$  and two 2 year floods in December with discharges fluctuating between  $698$  and  $1950 \text{ m}^3 \text{ s}^{-1}$ .

### 3.1. Field Measurements

#### 3.1.1. Multibeam Echosoundings

Multibeam echosoundings were performed with an Odom ES3 echosounder containing 240 sensors transmitting at a frequency of 240 kHz and opened to a width of  $120^\circ$ . With this configuration, the riverbed is scanned over a width equal to three times the water depth. The echosounder was associated with a DGPS ProFlex 500 (Magellan), which ensures a centimetric accuracy in the planimetric and vertical planes. Measurements were performed in longitudinal tracks parallel to the banks at a boat velocity between  $1.5$  and  $3 \text{ m s}^{-1}$ . Between 5 and 8 h (depending on flow conditions), representing  $\sim 70$  longitudinal tracks, were necessary to cover the whole study reach. The multibeam bathymetric data were postprocessed with Hypack 2009 software in order to filter the multibeam bathymetric data and convert them to  $0.5 \text{ m}$  grids (composed of an average of 550,000 points). This grid is then interpolated by triangulated irregular network (TIN) in ArcGis (9.3) to produce Digital Elevation Models (DEMs) and thus to fill in gaps between longitudinal tracks. To spatialize the zones of deposition and erosion, DEMs are differentiated with spatial analyst in ArcGis (9.3) to construct DEMs Of Difference (DoDs).

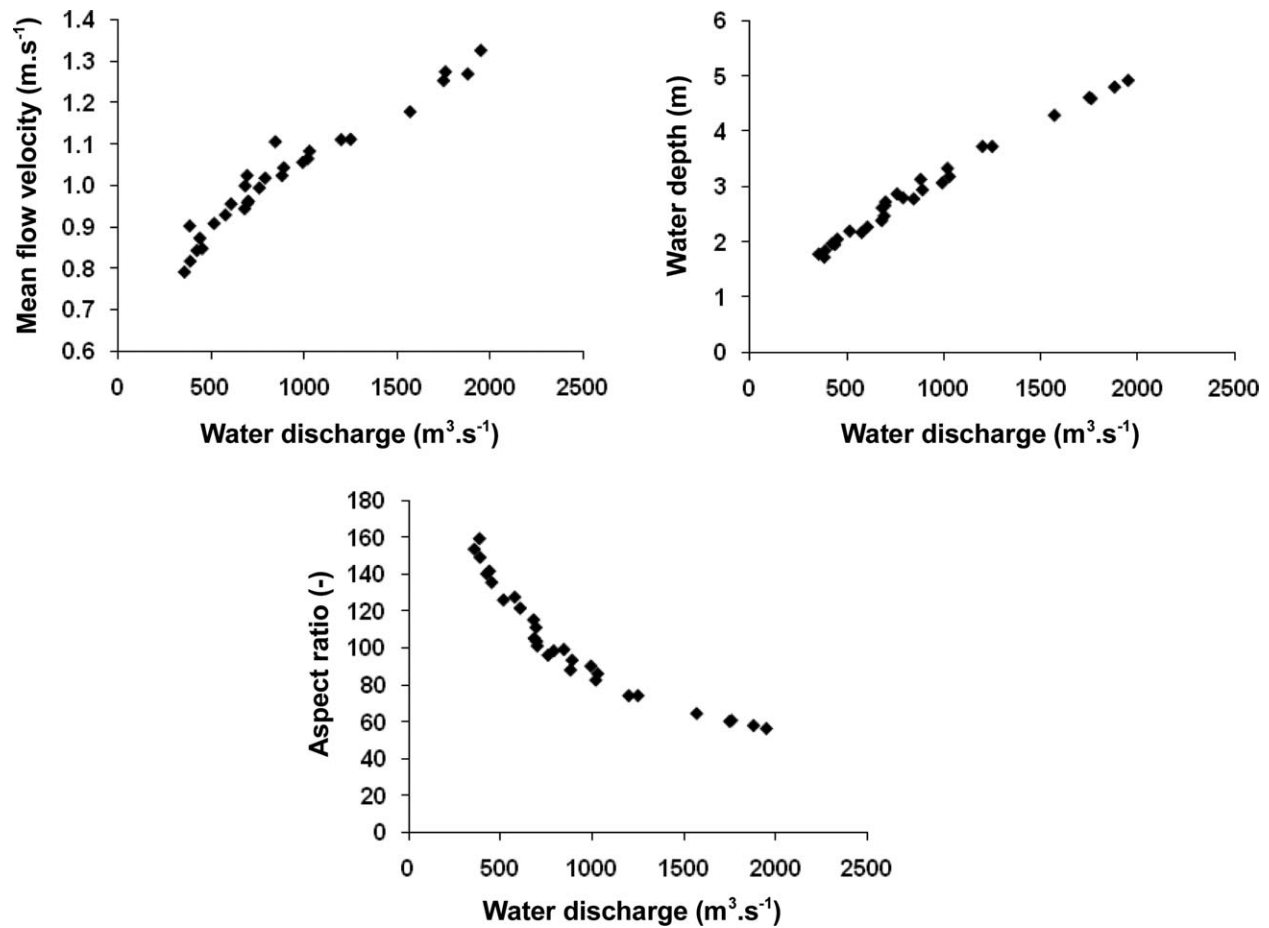


Figure 2. Evolution of the mean hydraulic parameters on P80 as a function of the water discharge.

### 3.1.2. Acoustic Doppler Profiler Measurements

Flow velocity measurements were collected with an ADP Sontek RiverSurveyor M9 on the boat used for the echosoundings. The ADP contains two sets of four profiling beams (one set at 3 MHz and one set at 1 MHz) and a low-frequency echosounder (0.5 MHz) to accurately measure the water depth. With the two acoustic

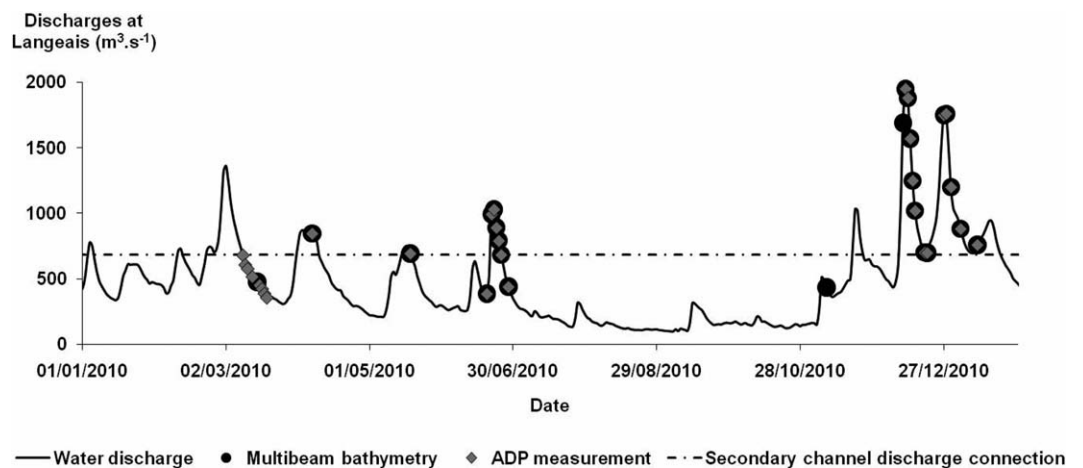


Figure 3. Distribution of the measurements on the hydrograph of the Langeais gauging station (4.5 km upstream from the study site).

**Table 1.** Absolute Median Error and Percentage of Values Exceeding the Error for the Flow Components  $u_E$ ,  $u_N$ , and  $u_V$  as a Function of Number Transects Averaged

Number of Transects	$u_E$		$u_N$		$u_V$	
	Absolute Median Error ( $\text{m s}^{-1}$ )	Percentage of Values Exceeding the Error (%)	Absolute Median Error ( $\text{m s}^{-1}$ )	Percentage of Values Exceeding the Error (%)	Absolute Median Error ( $\text{m s}^{-1}$ )	Percentage of Values Exceeding the Error (%)
1	0.027	100.00	0.025	98.27	0.010	44.67
2	0.018	100.00	0.021	98.37	0.005	71.93
3	0.012	100.00	0.012	98.43	0.004	80.31
4	0.006	100.00	0.007	99.48	0.002	88.48

frequencies, the device automatically adjusts to the appropriate acoustics and pulse schemes as a function of the hydraulic parameters (flow depth and velocity) encountered during the survey. The bin height is automatically adjusted on each vertical as a function of the water depth. The distance from the water surface to the first bin varies with the water discharges between 0.50 and 0.85 m. The last bin is located at least at 6% of the water depth above the river bed. The flow velocities are defined in every bin by the easting ( $u_E$ ), northing ( $u_N$ ), and vertical components ( $u_V$ ). Onboard the boat, the DGPS (Magellan ProFlex 500) was connected to Hypack 2009 software to ensure that most of the ADP tracks were located at a maximum of 1 m from the cross section. With this field protocol, the data provided by the ADP compass and bottom tracking ensure that the velocity measurements are accurately positioned.

Three cross sections (P80, P90, and P95) were monitored daily during the surveys (Figure 1). To conduct the echosoundings and ADP measurements in a single day, two transects were performed on each cross section at a boat speed of  $\sim 1 \text{ m s}^{-1}$ . In postprocessing, the flow velocities ( $u_E$ ,  $u_N$ ,  $u_V$ ) and water depth recorded from the two transects performed on a cross section were projected on a grid with cells of 5 m width and height equal to the maximum height of the bins defined during the measurements [Dinehart and Burau, 2005a, 2005b]. A mean value of the flow velocities components was calculated in each cell of the grid. Then the horizontal flow velocity,  $u$  (equation (1)) and its orientation with respect to north  $\varphi$  are estimated in each cell.

$$u = (u_N^2 + u_E^2)^{0.5} \quad (1)$$

As five transects are recommended per cross section [Szupiany *et al.*, 2007], we verified if the average of two transects can give values of the three flow velocities components sufficiently close to those estimated with five transects. For this purpose, we had available of five transects performed on the cross section P80 on the 11 March 2010. On a grid composed of 384 cells, the average cross sectional values of  $u_E$ ,  $u_N$ , and  $u_V$  computed by the average of five transects were 0.91, 0.21, and  $-0.045 \text{ m s}^{-1}$ , respectively. For the three components, we estimated in each cell, the difference between the mean value obtained from 1, 2, 3, and 4 transects, and the value obtained from five transects. The absolute median errors for each component are presented in Table 1. We see that with an average of two transects, the absolute median error represents 10% of the average cross-sectional values of  $u_N$  and  $u_V$ , and only 2% for  $u_E$ . Then the number of values in the grid that exceeds the absolute median error was computed. Even with one transect, 100% and 98% of the values calculated for the horizontal components  $u_E$  and  $u_N$  were higher than the absolute median error (Table 1). Therefore, the mean of two transects could not lead to misinterpretation of horizontal flow structures. For the vertical component, with two transects, almost 72% of the averaged values were above the absolute median error of  $0.005 \text{ m s}^{-1}$  (Table 1). Thus, even though a small part of the vertical velocities could be directed toward the wrong direction, the average of two transects could be sufficient to correctly describe the large flow structures observed with an average of five transects. This finding is coherent with an estimation of the accuracy of flow velocities obtained from two transects by cross sections on the Colorado River by Wright and Kaplinski [2011].

The accuracy of the horizontal flow velocity ( $u$ ) was assessed by comparing them to vertical velocity profiles obtained by a current meter OTT C31. With this device, the velocities were collected for 30 s near the riverbed, near the surface and at 20, 40, 60, and 80% of the water depth. At each level, measurements were repeated six times. The mean bias and dispersion (i.e., the standard deviation of the error) calculated over 27 verticals for six dates were  $-0.024 \text{ m s}^{-1}$  and  $0.091 \text{ m s}^{-1}$ , respectively. The randomness of the errors between the current meter and ADP data and the normality of their distribution was investigated by means of the Shapiro-Wilk test that is adequate in case of small number of samples ( $n < 50$ ). This test indicates that

the null hypothesis ( $p$  value = 0.71) cannot be rejected, i.e., that the error distribution is likely to be normal and random. The mean standard error for each individual flow velocity measurement was  $0.094 \text{ m s}^{-1}$ . The biases with respect to current meter measurements were maximum for low flow velocity ( $-0.08 \text{ m s}^{-1}$  on average for flow velocity  $< 0.87 \text{ m s}^{-1}$ ) that were observed under shallow water depth conditions but remained very limited otherwise. Therefore, low flow velocities obtained by ADP should be regarded with care. Cross sectional mean river depths obtained by ADP agree to field measurements within an average of 7.5%. This low precision might essentially be attributed to the mismatch of the boat position for both measurements. As a conclusive test, it must be remarked that the relations linking flow velocity and river depth, based on ADP and current meter, are mutually very consistent, marked by a flow velocity baseline value comprised between  $0.62 \text{ m s}^{-1}$  and  $0.64 \text{ m s}^{-1}$  and a gain of  $0.14 \text{ m s}^{-1}$  for each additional meter of river depth. The uncertainty of river discharge inferred from ADP was calculated by propagation of the components errors [Cornell, 1972] and found to be comprised between 3 and 10% over the six cross sections investigated at the 95% confidence level. The contributions of the river cross section (mainly river depth) and the flow velocity to the uncertainty relative to the river discharge are of same magnitude (45% versus 55% on average). However, it is probable that the uncertainty associated to the river depth is overestimated because of the mismatching between current meter and ADP measurements.

### 3.2. Primary and Secondary Components of Flow Velocities

In rivers, flows are rarely parallel to the banks and can follow a direction oblique to the longitudinal slope. To filter the lateral component of flows, it is often necessary to reorient velocity vectors to obtain the primary (parallel to the mean direction vectors) and secondary (perpendicular to the mean direction vector) current velocity components [McLelland *et al.*, 1994].

However, in large rivers, the direction of velocity vectors is generally not uniform along a cross section because of the divergence or convergence of flow within the bed. This phenomenon is particularly true in areas of confluence, bifurcation, or sudden narrowing and widening of the channel. Most methods that define the orientation of primary velocities were defined for small streams in which the directions of the vectors can be considered invariant across the width of the channel [McLelland *et al.*, 1994; Lane *et al.*, 2000]. These methods, which use only one plane to determine the direction of the primary and secondary components across the width of a channel, are not applicable to large rivers [Szupiany *et al.*, 2009]. Thus, it seems preferable to use methods such as the one defined by Rozovskii [1954]. This method defines a primary flow direction for each vertical equal to the mean direction of the vertical velocities. The directions of the primary ( $u_p$ ) and secondary ( $u_s$ ) components at any point of a section are obtained from the difference between the depth-averaged direction of the velocity and the direction of the vector at the point concerned. The components  $u_p$  and  $u_s$  are then calculated:

$$u_p = u \cos(\varphi - \psi) \tag{2}$$

$$u_s = u \sin(\varphi - \psi) \tag{3}$$

where  $u$  is the flow velocity at each vertical cell,  $\varphi$  is the orientation of the vector  $u$  with respect to north, and  $\psi$  is the orientation of the mean vector velocity on the vertical with respect to north.

In this study, the secondary currents or helical currents are defined as flows extending over several verticals with secondary velocities ( $u_s$ ) on the surface and near the bed directed toward the opposite banks [Rhoads and Kenworthy, 1995; Szupiany *et al.*, 2009].

### 3.3. Bed Shear Stress

The bed shear stress,  $\tau$ , is defined in relation to the current velocity profile and the law of the wall.

$$\tau = \rho \left[ \frac{\kappa u}{\ln\left(\frac{z}{(z_0)_{SF}}\right)} \right]^2 \tag{4}$$

where  $\rho$  is the volumetric mass of water ( $1000 \text{ kg m}^{-3}$ ),  $u$  is the current velocity at height  $z$  over the bed top,  $\kappa$  is the von Karman constant equal to 0.4 for clear water, and  $(z_0)_{SF}$  is the grain roughness (or the

height at which  $u = 0$ ), equal to  $0.095 D_{90}$  [Wilcock, 1996]. The adjustment made by linear regression between the values of  $u$  and  $\ln(z)$  measured on a vertical allow for the estimation of the element contained between the square brackets in equation (4) and thus for the  $\tau$  on the vertical [Sime et al., 2007; Szupiany et al., 2007, 2009; Rennie and Church, 2010].

The critical bed shear stress,  $\tau_c$ , is calculated from the Shields curve [Van Rijn, 1984]:

$$\text{for } 20 < D_* < 150 \quad \tau_c = 0.013 D_*^{0.29} (\rho_s - \rho) g D_{50} \quad (5)$$

where  $D^*$  is the nondimensional diameter,  $\rho_s$  is the volumetric mass of sediment ( $2650 \text{ kg m}^{-3}$ ),  $\rho$  is the volumetric mass of water ( $1000 \text{ kg m}^{-3}$ ), and  $g$  is the gravitational acceleration ( $9.81 \text{ m s}^{-2}$ ).  $D_*$  is defined by:

$$D_* = D_{50} \left( \frac{(s-1)g}{\nu^2} \right)^{\frac{1}{3}} \quad (6)$$

$D_{50}$  is the diameters for which 50% of the particles in weight are finer,  $s$  is the sediment density ratio (2.65), and  $\nu$  is the kinematic viscosity ( $1 \times 10^{-6} \text{ m}^2 \text{ s}^{-1}$ ).

### 3.4. Dimensions of Bed Forms

The heights ( $H_D$ ) and wavelengths ( $L_D$ ) of the dunes are calculated using the Bed form Tracking Tool Matlab code [for further description, see Van der Mark et al., 2008] on 100 m long longitudinal topographic profiles that are positioned every 25 m along the three transverse profiles followed by ADP (Figure 4). These profiles are taken from elevation maps obtained from multibeam bathymetric data. On 9 March 2010, topographical profiles were extracted from four longitudinal profiles measured by a single-beam echosounder.

### 3.5. Bed Roughness Associated to Dunes

The total bed roughness is commonly divided into two components: a grain roughness referring to the resistance to flow due to the shear stress applied on the grains of the river bed and a form roughness referring to the resistance to flow due to the pressure differential and energy loss in turbulences on the lee side of bed forms [Julien et al., 2002]. However, the bed roughness of the main channels is mainly influenced by the form drag (due to the dunes) in sand, gravel, or sand-gravel bed rivers [Paarlberg et al., 2010]. To observe the spatial distribution of the bed roughness, the component due to the dunes ( $ks$ ) is estimated using the Van Rijn's [1984] approach:

$$ks = 1.1 H_D \left( 1 - e^{\left( -25 \frac{H_D}{L_D} \right)} \right) \quad (7)$$

where  $ks$  is the bed roughness associated to the dunes (m),  $H_D$  is the mean dune height (m), and  $L_D$  is the mean dune length (m).

## 4. Results

### 4.1. Morphological Evolution of Bars

In the channel expansion/contraction examined, the bed topographies measured between March and December 2010 show that bars adopted different configurations (Figure 5). Indeed, the macroforms presented successively an alternate, a lateral and a transverse pattern.

On the first survey, on 15 March 2010 (Figure 5a), two bars, B1 and B2, superimposed by dunes, are positioned in alternate configuration and separated by the pool P1. The bar B1, located near the right bank, measures 555 m long and 1.69 m high (Table 2). Further upstream and close to the other side, the bar B2 also reaches 1.69 m high (the area monitored is too short to measure the length of B2).

On 18 May 2010, DEM (Figure 5b) and DoD (Figure 6a) show that B2 has migrated 180 m downstream parallel to the left bank at an average velocity of  $2.2 \text{ m d}^{-1}$ . This migration speed is equivalent to that observed

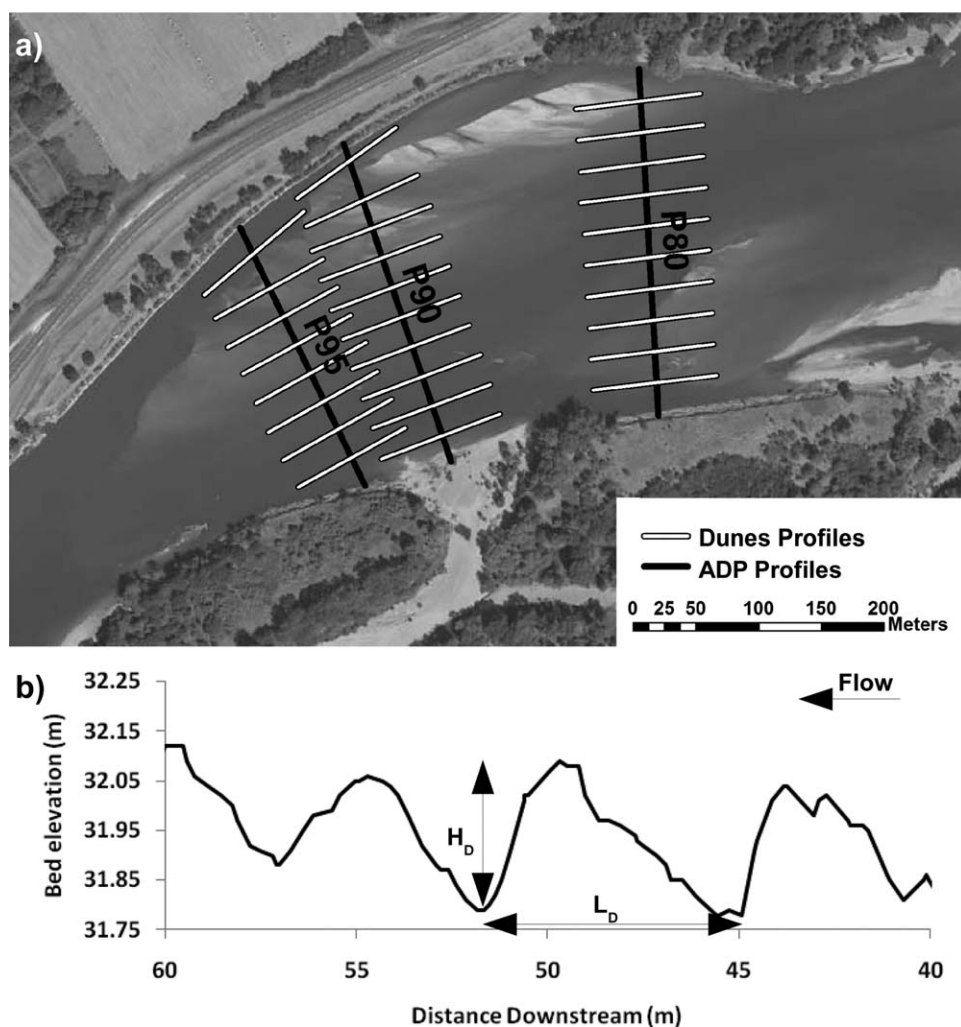


**Figure 4.** (a) Location of the profiles used to determine the dunes characteristics and (b) definition of dune height and dune wavelength.

on other sites on the Loire River [Rodrigues *et al.*, 2012]. The progradation of B2 results in the migration to the right bank of the pool P1 and in the erosion of part of B1. This pattern of macroforms is then named lateral bar configuration in the following sections. A unit bar, UB1, 90 m long, also appears at the head of former bar B1 by the accretion of large dunes entering in the system through the forced pool FP1 (Figures 5b and 6a). In this study, a unit bar is defined as a bar having a shape that remains relatively unmodified during migration and being a simple form that is not amalgamated or superimposed upon other bars [Smith, 1978].

Between 18 May 2010 and 19 June 2010, the downstream part of B1 is completely eroded (Figure 5c). B2 migrates laterally toward the center of the main channel (at an average velocity of  $2.3 \text{ m d}^{-1}$ ) and merges with UB1 which progrades in a downstream direction (Figure 6b). The merged or compound bar (B2) shows a well-marked transverse configuration at the center of the main channel. A compound bar corresponds to a form that comprises more than one unit bar and evolves through several erosion and deposition events [Bridge, 2003]. During the flood of June, the compound bar B2 measures between 545 and 570 m long, and between 1.41 and 1.63 m high (Table 2). The reattachment of B2 to the right bank (by merging of B2 with UB1) enables the formation of a new pool, P2, between the transverse bar and the left bank. At the beginning of the flood (Figure 5c), a new unit bar, UB2 migrates in P2. At the end of the event (Figure 5d), the unit bar UB2 is close to reach the compound bar B2. This observation could indicate that unit bars continue to aggregate to the large bar B2. The DeMs and DoD obtained from the echosoundings (Figures 5c, 5d, and 6c) indicates that during the flood of June, the bed evolutions are mainly attributed to dunes dynamics, to

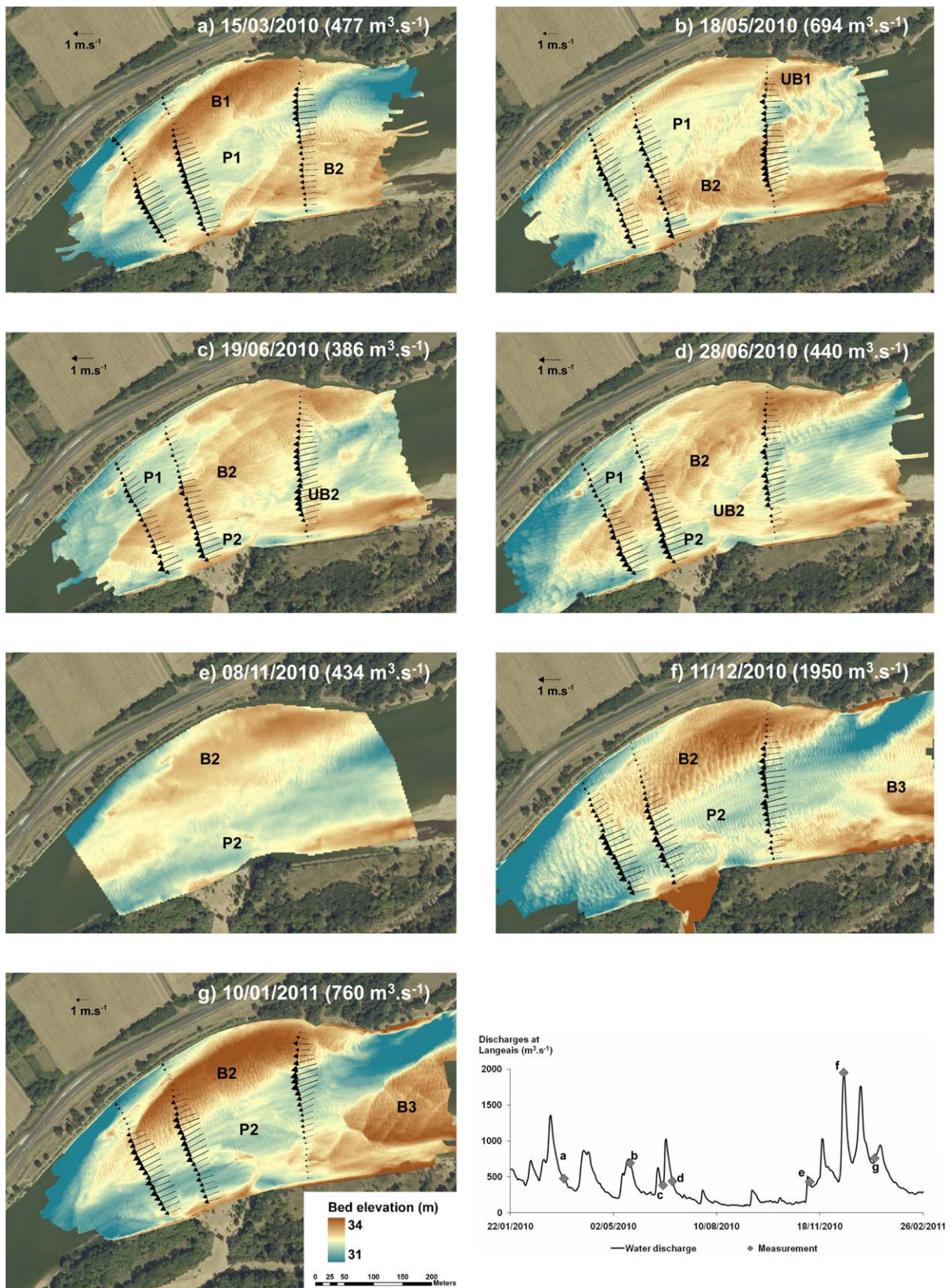


**Figure 5.** Bars configuration and associated depth-averaged flow velocities for 7 different surveys in 2010 (a, b, c, d, e, f, and g). Note that the flow velocities presented for the 15/03/2010 are those measured on the 09/03/2010 at 681 m<sup>3</sup> s<sup>-1</sup>. See text for notations.

**Table 2.** Length and Height of Bars<sup>a</sup>

Date	B1		B2		B3	
	Length (m)	Height (m)	Length (m)	Height (m)	Length (m)	Height (m)
3/15/2010	555	1.69	b	1.69	c	c
5/18/2010	535	1.29	360	1.08	c	c
6/19/2010	c	c	545	1.41	c	c
6/28/2010	c	c	570	1.63	c	c
12/11/2010	c	c	500	1.87	b	1.58
1/10/2011	c	c	520	2.20	b	1.63

<sup>a</sup>HB is equal to the average height measured on the three transverse profiles.  
<sup>b</sup>Data not available.  
<sup>c</sup>Bars not present on the study site.

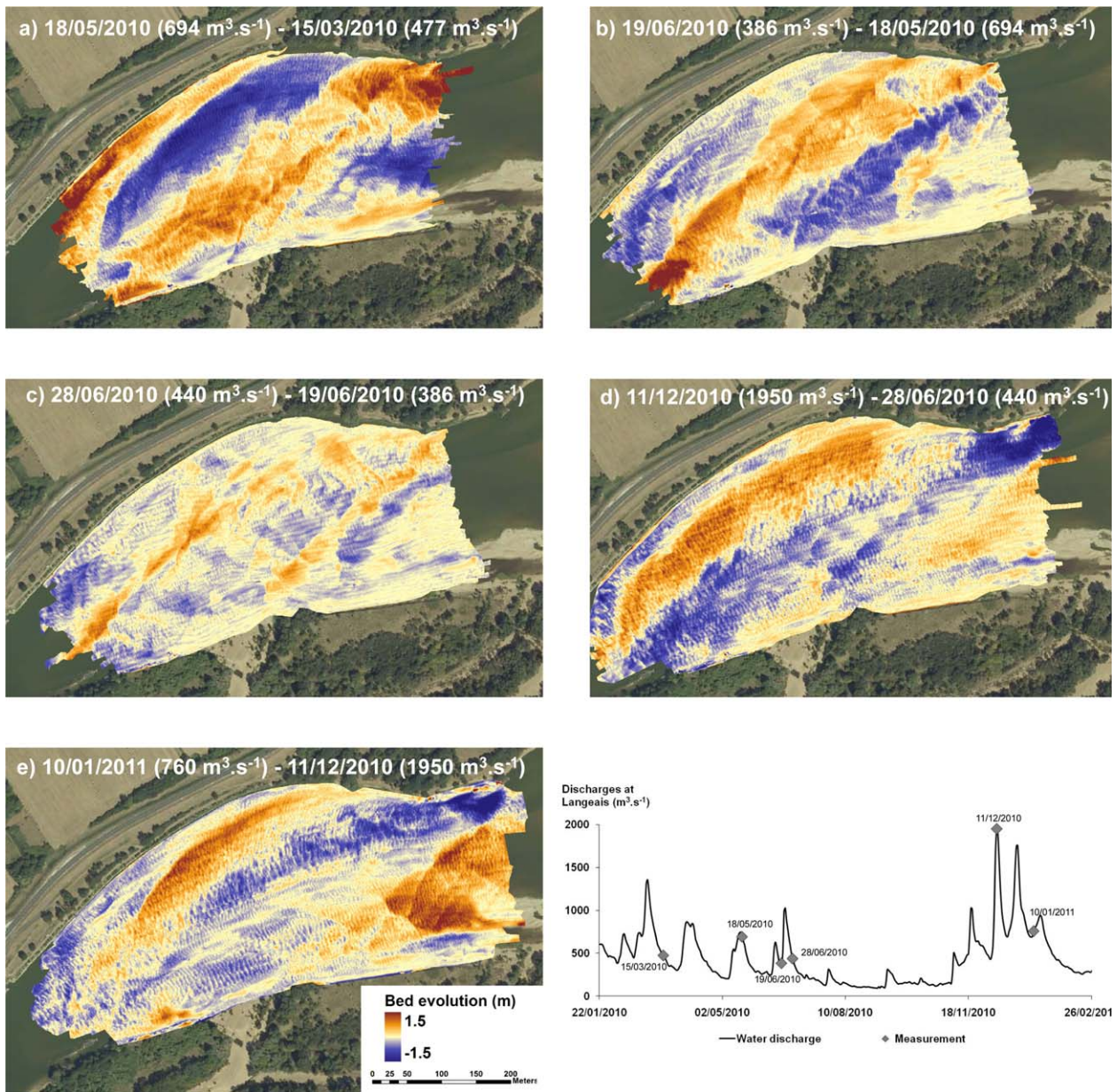


Figure 6. Topographical evolution of the bed river between the surveys presented in Figure 5. The letters a, b, c, d, e, and f refer to the 6 differential maps.

the unit bar progradation and to the lateral migration of the transverse bar (from the left toward the right part of the channel).

On 08 November 2010, at the end of the low flow period of the summer and before the first wintery flood, the bar B2 has finished its transverse migration and reached the rip-raps, R1, near the right bank (Figure 5e). This observation indicates that in this sandy-gravel bed river, the bars' morphodynamic is still active during low flow periods [Kiss and Sypos, 2007].

On 11 December 2010, at the beginning of the floods of December, a new configuration of alternate bars is in the process of being formed following the appearance of a new bar, B3, upstream near the left bank and the previous attachment of B2 to the right bank (Figures 5f and 5g). The main bed evolutions observed during these events are attributed to dunes dynamic, to the lateral migration of B2 (toward the right bank) which becomes higher and less wide and to the downstream progradation of B3 (Figure 6e). The length of B2 varied between 500 and 520 m and its height between 1.87 and 2.20 m. The height of B3 fluctuates around 1.60 m.

#### 4.2. Primary Velocities

The primary velocities are presented in Figure 7. For the lower discharge ( $386 \text{ m}^3 \text{ s}^{-1}$  on 19 June 2010), the primary velocities vary between  $0.34$  and  $1.31 \text{ m s}^{-1}$  and for the higher discharge ( $1950 \text{ m}^3 \text{ s}^{-1}$  on 11 December 2010) they fluctuate between  $0.48$  and  $1.72 \text{ m s}^{-1}$ . The results of the surveys performed during the floods of June (Figures 7c and 7d) and December (Figures 7e and 7f) highlight that for a bar configuration, the distribution of the velocities changes moderately with the discharge. Figure 8 presents differentials of primary velocities acquired during three surveys. These measurements were performed at similar discharges ( $700 \text{ m}^3 \text{ s}^{-1}$ ) but on different bars configurations (alternate, lateral, and transverse bars). The differentials indicate that the zones with a decrease (in blue) or an increase (in red) of the velocities are positioned, respectively, according to the apparition or the disappearance of a bar. Thus, the macroforms slow down the flows on their tops. Note that for the lateral configuration (18 May 2010), the profile P80 is located on the upstream part of the bar B2 (Figure 5b). In this configuration, the influence of the bar in the left part of this cross section is not sufficient to reduce the velocities. So the speeds in the left part of the channel are higher than those observed on the alternate bar B2 (see Figure 5a and P80 in Figure 8a) and of the same order of magnitude than the velocities measured without macroform in this area (Figure 8c). The organization of the primary velocities is significantly controlled by the configuration of the bars in the channel expansion/contraction.

The analysis of the spatial distribution of primary velocities has highlighted two flow patterns corresponding to two bars configurations (Figure 7). First, when the macroforms are in an alternate configuration, on the three cross sections, high primary velocities flow are located in the pool in the center of the channel along the left edge of the bar situated near the right bank (Figures 7a, 7e, and 7f). These high velocities extend to the left bank on P90 and P95. The second flow pattern is observed for the transverse and lateral bar configurations. With these morphologies, in the expansion zone (P80), high velocities are located on the left part of the channel, on the bar B2 on 18 May 2010 and on the unit bar UB2 during the flood of June. Downstream on P90, in June, high velocities are deflected by the transverse bar B2 and constrained between the left bank and the macroform on the left part of the channel (Figures 7c and 7d). On this profile, for a lateral bar, high velocities are also observed on the right part of the channel (Figure 7b), which indicates that in this configuration, the flow is less constrained by the macroform than in a transverse pattern. Downstream, on P95, the flow velocities are more uniform on the cross section. However, the highest speeds are still located between the left bank and the bars.

For all bars configurations, the lowest primary velocities are located near the left and right banks on P80 and near the right bank on P90 and P95. On P95, the low velocities located close to the right bank tend to disappear with the increase of the water discharge.

The average flow velocities (Figure 9a) increase from upstream to downstream, i.e., inversely to the aspect ratio (Figure 9b). Additionally, the average primary velocities obtained from the measurements of 9 March 2010, 18 May 2010, and 25 June 2010 (performed at an equivalent discharge around  $700 \text{ m}^3 \text{ s}^{-1}$  and similar aspect ratios), are higher across lateral and transverse bars (18 May 2010 and 25 June 2010) than in an

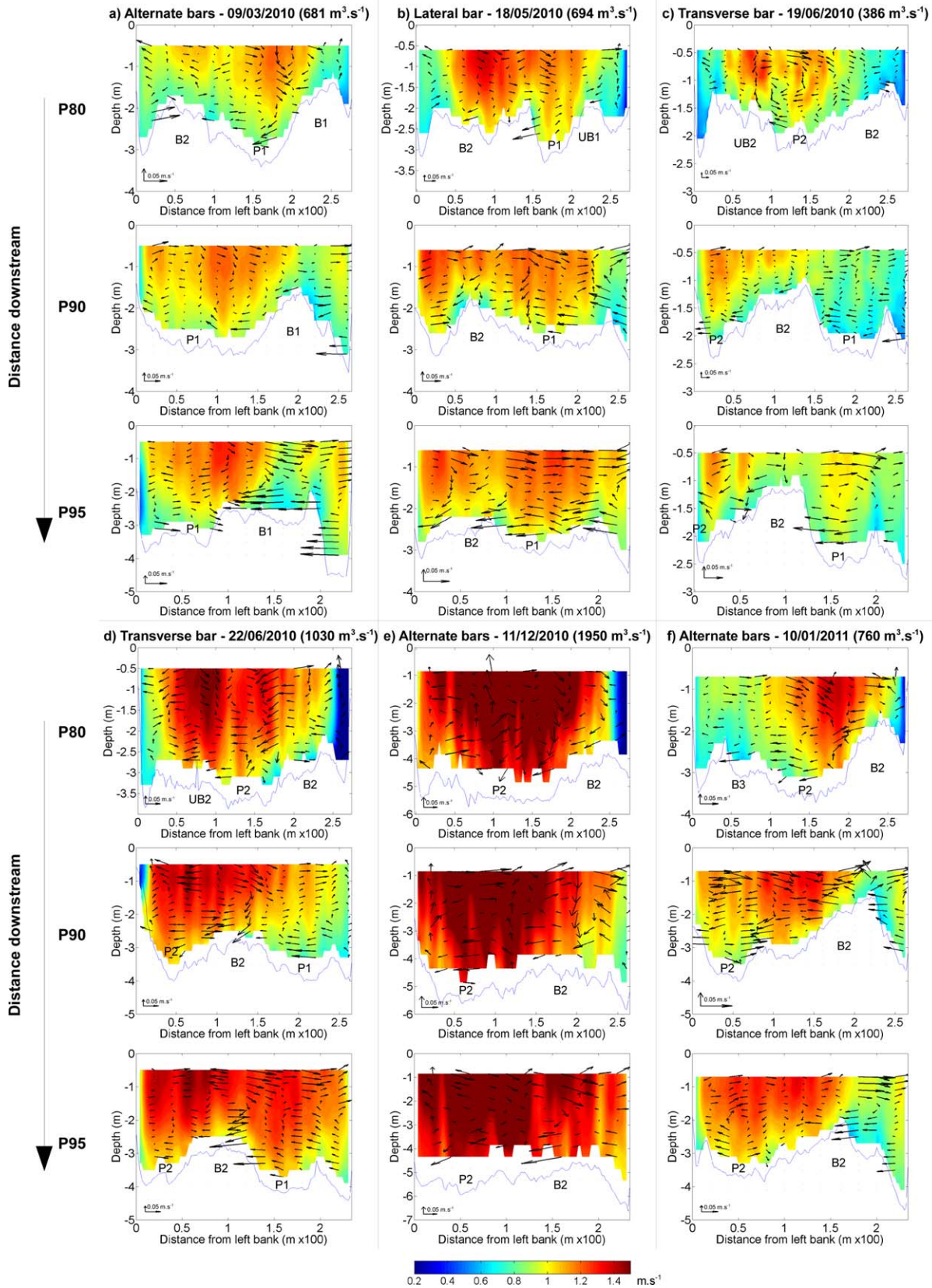


**Figure 7.** Primary, secondary, and vertical velocities on the profiles P80, P90, and P95 for 6 different bars configurations and flow discharges (a, b, c, d, e, and f). The filled contours are the primary velocities. The arrows indicate the secondary and vertical velocity components. The blue lines represent the topography of the river bed.

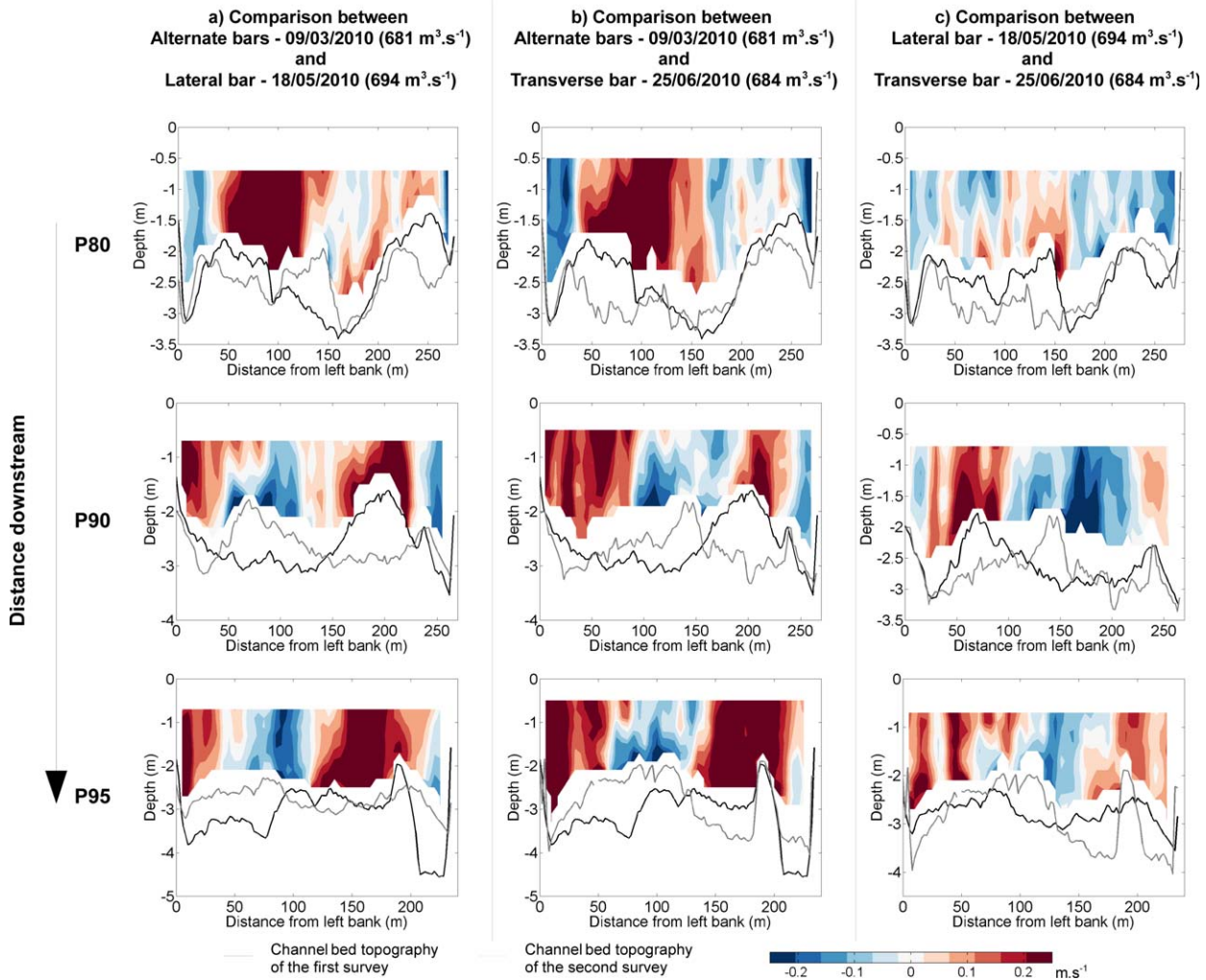


**Figure 8.** Differential of primary velocities between three surveys carried for similar water discharges and different configuration of bars. The differentials correspond to the primary velocities of the second survey minus those of the first survey. (a and b) The first survey corresponds to the measurements performed on the 9 March 2010. (c) The first survey corresponds to the data of the 18 May 2010.

alternate bars configuration (9 March 2010). Thus, the averaged flow velocities at  $694 \text{ m}^3 \text{ s}^{-1}$  in transverse bar configuration are only similar to those observed at  $760 \text{ m}^3 \text{ s}^{-1}$  with alternate bars configuration.

### 4.3. Secondary Velocities, Vertical Velocities, and Secondary Currents

The secondary ( $u_s$ ) and vertical ( $u_v$ ) velocities components are represented by the arrows in Figure 7. Lateral and vertical velocities have low values varying around  $0.1 \text{ m s}^{-1}$  and  $0.05 \text{ m s}^{-1}$ , respectively. These values are of the same order of magnitude than those observed in other alluvial systems [De Serres *et al.*, 1999; Nicholas and Sambrook Smith, 1999; Szupiany *et al.*, 2009, 2012; Kasvi *et al.*, 2013]. As a general observation, the analysis of the pattern of the secondary and vertical velocity vectors only exhibits two small structures.

First, on P80, for alternate bars configurations and on P90 on the 9 March 2010 (Figures 7a, 7e, and 7f), close to the bar located near the right bank, the velocity vectors of the surface are directed toward the right bank and dive toward the river bed on the edge of the macroform. This downdraft current can be associated to a deflecting effect of the bar, and causes a vertical recirculation of the flows in the central pool. The absence of clear updraft currents near the left bank does not allow considering this structure as a secondary current.

Second, on profiles P90 and P95, the secondary and vertical velocities are organized differently according to their location in the channel. Between the bar and the right bank, two layers can fairly well be distinguished. These layers are composed of large secondary velocities and small vertical velocities. Near the

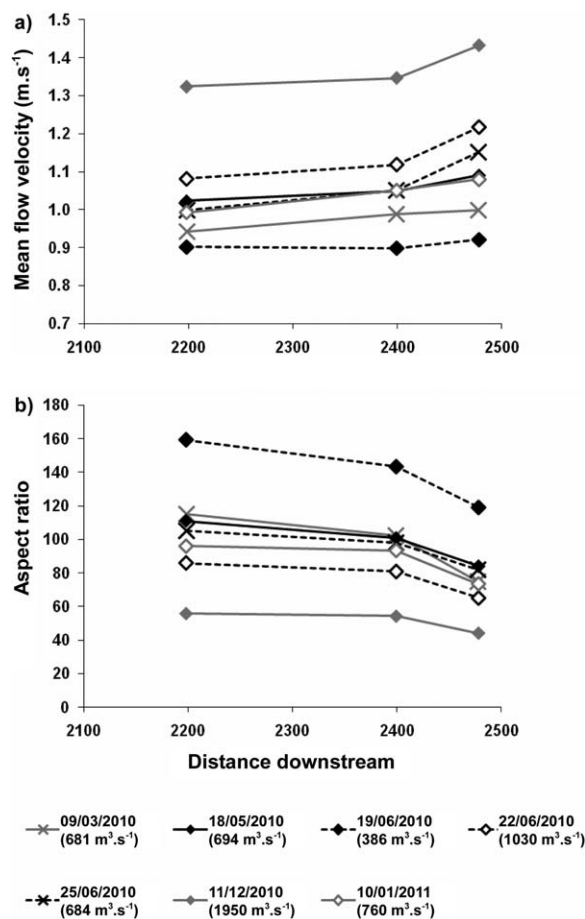


**Figure 9.** (a) Longitudinal evolution of cross-sectional averaged primary velocities and (b) aspect ratios. The gray lines designate the surveys with alternate bars. The black lines indicate the surveys with lateral or transverse bars.

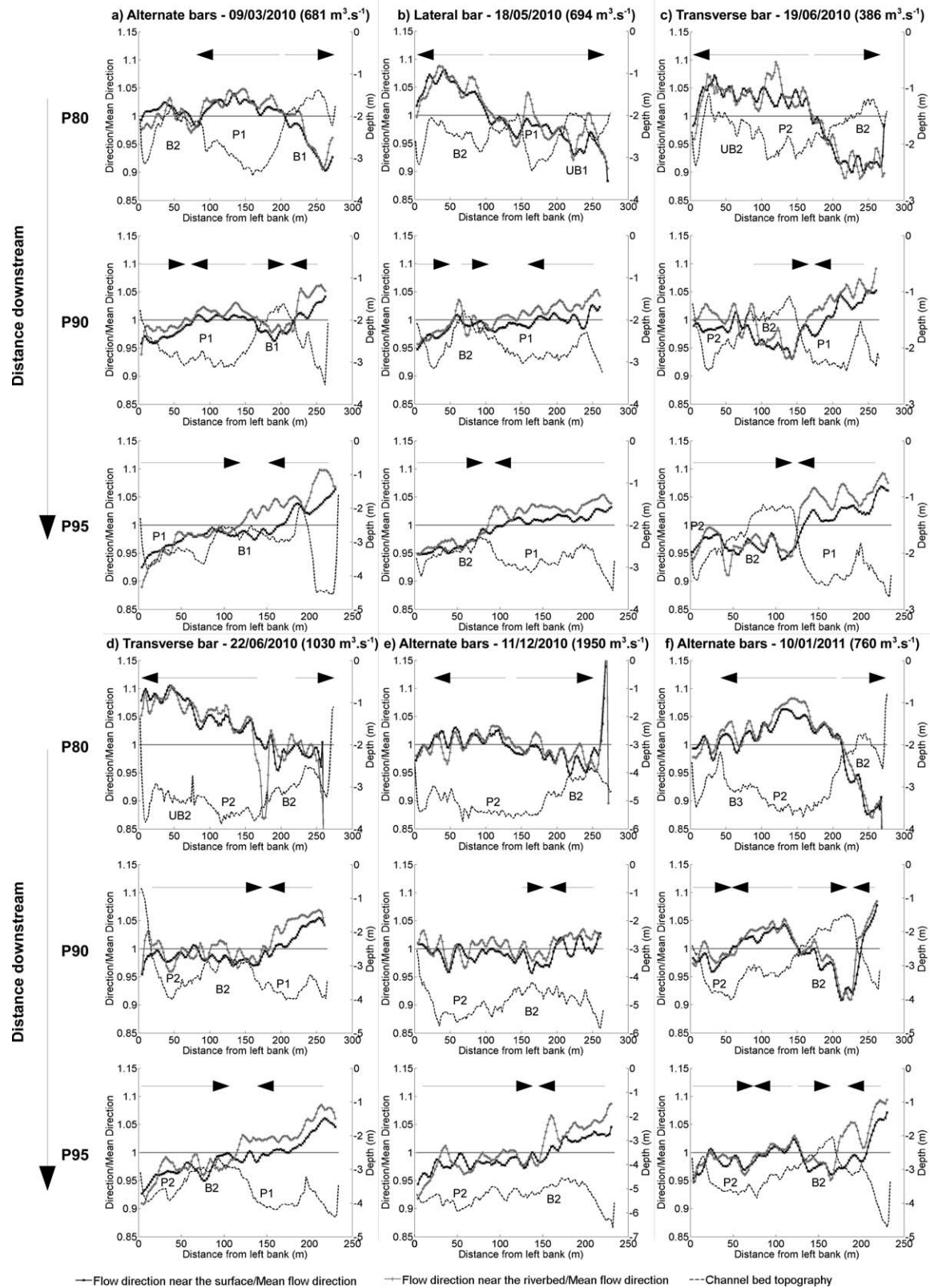
causes a small flow convergence, with the outer streamlines slightly directed toward the center of the channel.

Figure 10 presents the transversal distribution of the flow direction in the two upper bins near the surface and in the two last bins above the river bed. The height of two bins varies between 0.2 and 1 m according to the flow conditions. An analysis of these flow directions shows that the bars affect the streamlines (Figure 10). The transverse distribution of the flow directions indicates that the separation of the streamlines on P80 is located on the bar close to the right bank when the macroform is well developed (i.e., for alternate and transverse bars configurations) and the water discharge not too high (Figures 10a, 10c, 10d, and 10f). On the same profile for lateral bar configuration (Figure 10b), the unit bar UB1 on the right is too small, so the currents separate in the middle of the section on the large bar which migrates near the left bank. On P90, the macroforms constitute a physical boarder which separates a current located between the bar and the right bank and directed toward the left bank from other currents with other directions. Downstream, on P95, the contact area between the convergent current streams is always positioned at the pool-bar interface. On P90 and P95, the current located between the bar and the right bank presents a permanent pattern characterized by a difference of flow direction between the surface and the bottom. This flow structure corresponds to the secondary currents observed in Figure 7. On the same cross sections, for high bars and/or low discharges, i.e., when the relative height of the bars is large (P90 on Figures 10a, 10c, and 10f and P95 in Figure 10f), the macroforms deflect locally the flows on their top which enhances the physical separation of the currents on each part of the bar. Although the bars do not cause the divergence or convergence of flows, they seem to control the location of the separation and reattachment points of the currents in the main channel.

surface, the vectors are directed toward the right bank and those near the bottom are directed toward the left bank. Although, the vertical velocities do not exhibit a clear recirculation, we can assimilate this layered structure to a secondary current. On the other part of the channel (between the left bank and the bar), the two layers disappear and the velocities do not present large coherent structures. Thus, the macroforms ensure a physical separation of two different flows.

#### 4.4. Flow Direction

The depth-averaged direction of the flow shown in Figure 5 indicates that the streamlines mainly follow a streamwise direction for all water stages and bar configurations. Nevertheless, it can be observed that the bank direction and so the channel width variations influence locally the flow direction. Thus, the upstream channel expansion leads to a small flow divergence on P80, with water flow projected toward the right bank on the right side of the section. Downstream on P95, the channel contraction



**Figure 10.** Transversal distribution of flow direction for 6 different bars configurations and flow discharges (a, b, c, d, e, and f). The directions in black correspond to the ratio between the mean flow direction in the 2 upper cells near the surface and the cross-sectional averaged direction. The directions in gray correspond to the ratio between the mean flow direction in the 2 last cells above the riverbed and the cross-sectional averaged direction. When the ratio of directions is greater than 1 (horizontal gray line), the flows tend to be directed toward the left bank and vice versa. The black arrows indicate the direction followed by the flows.

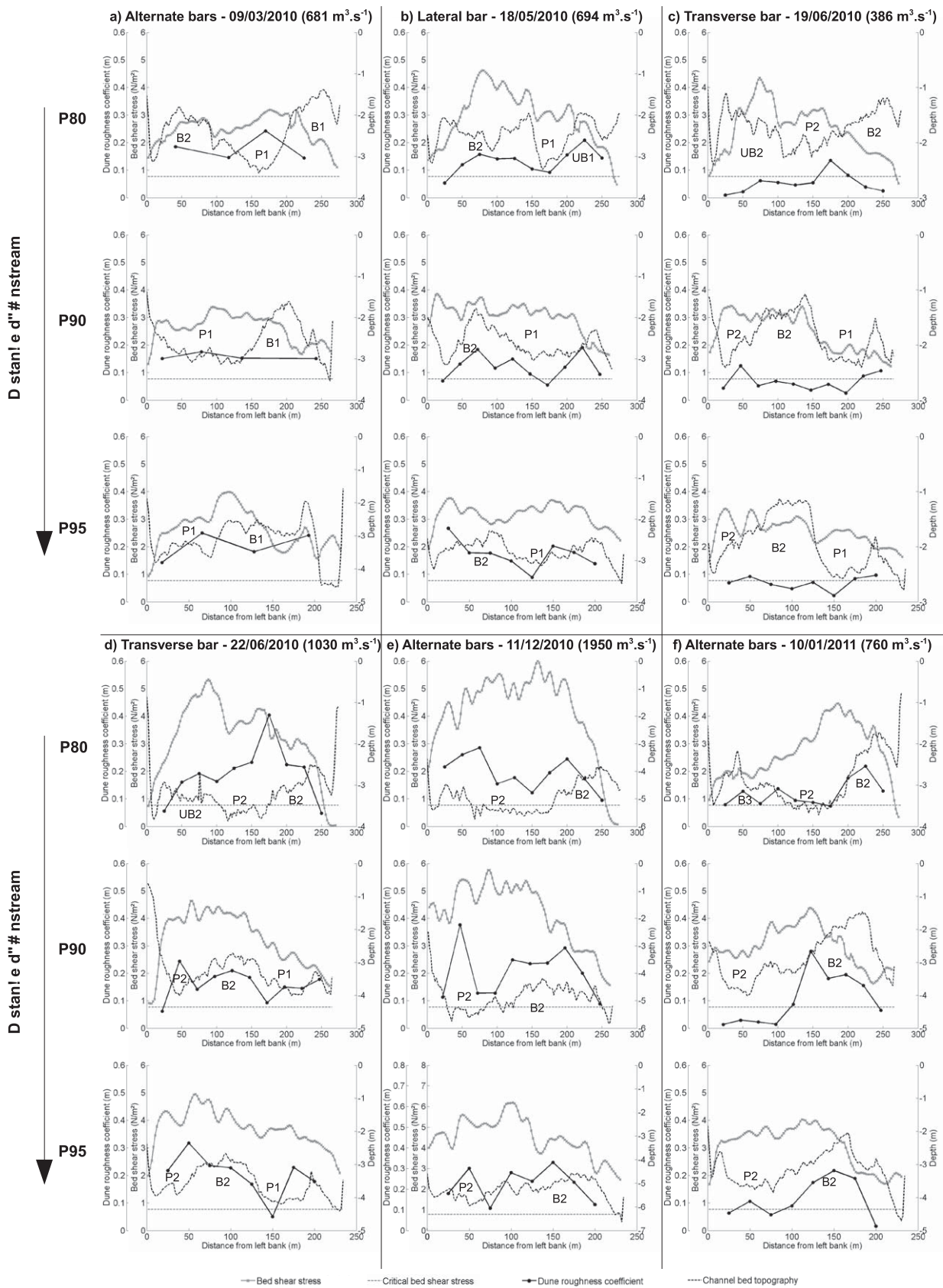
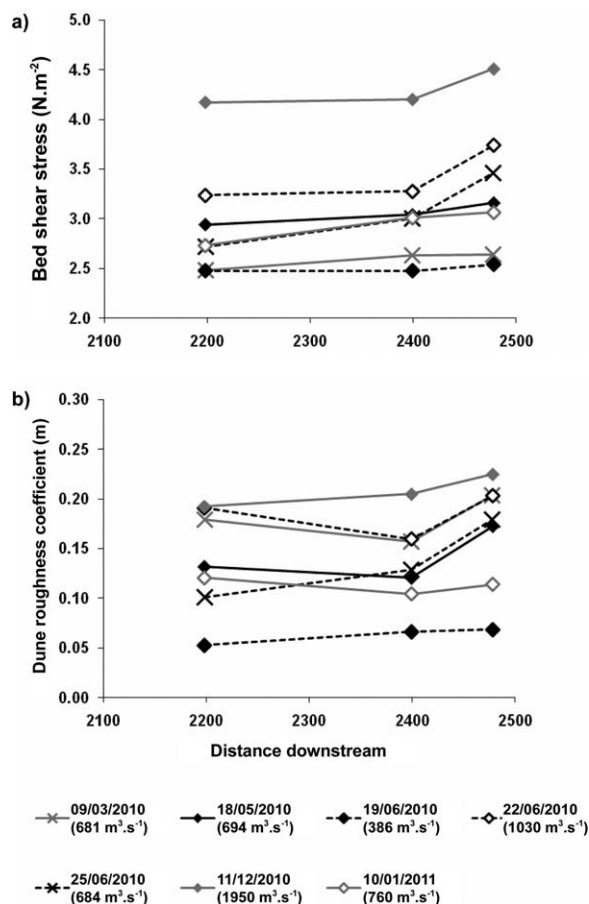


Figure 11. Transversal distribution of bed shear stresses and dunes roughness coefficients for 6 different bars configurations and flow discharges (a, b, c, d, e, and f).



**Figure 12.** Longitudinal evolution of the cross-sectional averaged (a) bed shear stresses and (b) dunes roughness coefficients. The gray lines designate the surveys with alternate bars. The black lines indicate the surveys with lateral or transverse bar.

**4.5. Bed Shear Stress**

Bed shear stresses ( $\tau$ ) estimated from equation (4) vary between 0.03 and 6.25 N m<sup>-2</sup> (Figure 11). The critical bed shear stress ( $\tau_c$ ) calculated from equation (5) reaches 0.78 N m<sup>-2</sup>. As observed in Figure 11, except a small part of the channel close to the right bank on P80, the bed shear stresses are significantly higher than the critical value. Whatever the water stages monitored, the sediments are highly mobile in the studied system. Nevertheless, the bed shear stresses are not uniformly distributed over the cross sections.

Upstream, on P80, in an alternate bar configuration for low discharges (Figures 11a and 11f), the bed shear stresses present the greatest values in the central pool P1, on the left edge of the bar located near the right bank. For higher discharges, the values of bed shear stresses are more uniform on the cross section (Figure 11e). For others configurations, on P80, the bed shear stresses are stronger on the bar close to the left bank. On P90, for alternate and transverse bars, the

strong bed shear stresses are located in the pool on the left side of the macroforms. Conversely, on this same profile, for lateral bar configuration (Figure 11b), the bed shear stresses are distributed more evenly over the section; in this case, the bar (B2) does not appear to affect the distribution of  $\tau$  in the channel. In the downstream profile (P95), large bed shear stresses are located between the left bank and the top of the macroforms with maximal values generally on the bar. In addition, on all profiles, the lowest bed shear stresses are located between the bars and the right bank.

Overall, as for primary velocities, cross-sectional averaged bed shear stresses increase from upstream (P80) to downstream (P95) especially between P90 and P95 in the contraction zone (Figure 12a), where the aspect ratio decrease significantly (Figure 9b). Moreover, for a same water discharge, the mean bed shear stresses are higher when the bars are transverse or lateral.

**4.6. Dunes Roughness**

The height ( $H_D$ ), the length ( $L_D$ ), and the roughness associated to the dunes ( $k_s$ , see equation (4) follow similar cross-sectional distributions. As the objective of this study is to observe the influence of the bed forms on the flows, the following part only focuses on the  $k_s$  parameter.

The roughnesses associated to the dunes are variables and fluctuates between 0.04 and 0.41 m (Figure 11). The higher values of  $k_s$  are found where the dunes are the highest, i.e., on the top or on the edge of the bars. Unlike what is generally observed in other systems, the largest dunes are located on elevated areas where the water level and flow rates are lower. Thus, the roughness is negatively correlated with flow depth, with the highest values in shallow areas, i.e., over the bars. This asymmetry of the cross-sectional

distribution of the dunes roughness coefficient is more marked for high discharges and during the falling limb of floods. Indeed, as seen on data in Figure 11c (which corresponds to low discharges conditions and to the beginning of a freshet) the  $k_s$  is relatively uniform along the cross sections. Additionally, on P90 and P95, on the measurements of December (Figures 11e and 11f), low dunes roughnesses are noticeable at 100 m and 75 m from the left bank, respectively. This decrease is attributable to the absence of dunes on the rip-raps R2.

The longitudinal evolution of the cross-sectional averaged dune roughness presents a general pattern which consists in a decrease of the  $k_s$  in the expansion zone followed by an increase in the contraction zone (Figure 12b). The mean dune roughnesses estimated for the 19 June 2010, the 25 June 2010, and the 11 December 2010 present a different feature characterized by a constant growth through the channel reach. Because of the lag time between discharge variations and dunes sizes, no clear relationship appears between cross-sectional averaged dunes roughness and bars configuration.

## 5. Discussion

According to the results, the configuration and morphology of the bars modify the flow structure already imposed by the right bank curvature, the channel width variations, and the forced units (bars and pools). This modifications on hydrodynamics, in turn, affects the bar morphodynamics and ensures a transition between the alternate and transverse configurations of bars in the channel expansion/contraction studied.

### 5.1. Influence of Bars on Flow Structures

Bars affect significantly the flow structure imposed by the planform, i.e., the channel expansion/contraction, the bank curvature, and the forced pools. The analysis of primary and secondary flow velocities (magnitudes and directions) and bed shear stresses has shown that in the expansion area studied (between P80 and P90), two flows with different features are located on each side of the bars at all water discharges. The widening of the channel causes a flow separation [Repetto *et al.*, 2002] which leads to the formation of two currents (see arrows in Figures 5 and 10). The main current with high primary velocities, high bed shear stresses and unstructured secondary velocities flows on the left part of the channel between the left bank and the bars. The absence of secondary currents in this flow is probably due to the straight pattern of the left bank and to the large aspect ratio associated to this part of the channel [Yalin and Selim, 1992; McLelland *et al.*, 1999]. The small current with low primary velocities, low bed shear stresses, and a secondary current is located between the bars and the right bank. The secondary current observed in the right part of the channel is probably induced by the curvature of the right bank. In the upstream part of the expansion zone, the divergence point between these two currents is found on the edge of the bars at all flows (see P80 in Figure 10). For low discharges and high bars (i.e., when the relative height of the bars is high), the divergence point extends downstream on the top of macroforms (see P90 Figures 10a, 10c, and 10f). Thus, the bars delimit and increase (at low flows) the divergence of the two currents induced by the upstream channel expansion. This influence of the macroform on the flow is similar to the topographic forcing described for point bars [Dietrich and Smith, 1983] and midchannel bars [Richardson *et al.*, 1996].

In alternate bar configuration, the deflection of the flow by the bars is also clearly visible with the macroforms located in the left part of the channel, in the narrow section upstream the expansion zone (see B3 in Figures 5f and 5g). In this morphological configuration, the highest flow velocities are deviated by the upstream bar toward the right bank and the left edge of the downstream macroform (see B2 in Figures 5f and 5g and P80 in Figures 7a and 7f). When bars are not upstream the expansion area (in transverse or lateral bars configuration), the high velocities are no more deflected toward the opposite bank and flow on the left part of the channel (Figure 5 and see P80 in Figures 7b, 7c, and 7d).

Downstream, in the contraction zone (between P90 and P95), the narrowing of the channel forces the convergence of the two currents induced by the upstream expansion zone. The contact point of these flows is located on the top or on the edge of the bars at all discharges (see P95 in Figure 10). The pressure gradient between the pool and the bar may be sufficient to form a shear layer between the two convergent flows in a manner similar to what is generally observed in confluences [Best, 1987; Biron and Lane, 2008]. This shear layer contributes to separate the two flow cells formed in the upstream expansion zone and reduce their mixing.

As mentioned before, the influence of bars on the flows is mainly due to a topographic forcing. Nevertheless, in the study site, at medium and high discharges, the large dunes and so the large dune roughness coefficients (according to the equation (7)) are generally located on the top or on the margin of the macroforms (Figure 11). *Parsons et al.* [2007] and *Szupiany et al.* [2009] showed that in sandy rivers with a high aspect ratio, large dunes can dampen the formation of secondary currents. Thus, the large dunes superimposed on bars could increase turbulence and prevent the development of the large-scale flow structures as the secondary currents (Figure 7) on the whole cross section. The large dunes could enhance the topographic forcing of the macroforms and contribute to maintain the separation of the two currents (with different characteristics) on each side of the bars. The bars associated to the large dunes trigger the nonuniformity of the flows in the channel.

## 5.2. Bars Morphodynamic in the Channel Expansion/Contraction

### 5.2.1. Bars Initiation Upstream Channel Expansion

A perennial forced pool, FP1, is located upstream the expansion area. Bed load seems to pass through the forced pool only as dunes since no macroform is observed in FP1. The bars generally enter in the system on the left part of the channel (B3, UB2 in Figures 5 and 6) or close to the right bank in the flow divergence area (UB1 in Figures 5 and 6). The location of the entering bars (i.e., in the left or right part of the channel) is always opposed to the position of the downstream macroform. Unit bars were observed in the channel during low flow periods just before floods (see UB2 in Figures 5c and 6b). Thus, high discharges do not seem to be the condition *sine qua non* for the entering of unit bars in the system. Nevertheless, the large bar (B3) appeared during 2 year floods. Floods (associated with large sediment supply) could be necessary to promote the large bar formation at the entrance of the system. The field data presented in this study are not sufficient to explore deeply the relations between bars entrance/formation and flow discharge. More investigations are needed to see if the large migrating bars only formed on the left part of the channel during high flows.

### 5.2.2. Discharge Variations Do Not Affect the Bars Migration

Once the bars are located in the channel expansion/contraction, their morphology changes all along the year (Figure 5), even during low flow periods because of the high mobility of the sediments (Figure 11) [Claude *et al.*, 2012]. This observation is relatively common in sandy rivers [Ashworth *et al.*, 2000; Kiss and Sypos, 2007]. Although some complex processes of fills and scours occur during the different stages of the freshets [Claude, 2012], the lateral migration of the bars (from the left to right bank) observed during the floods of June and December seems to be a continuous phenomenon (Figures 5 and 6). This lateral moving is also observed at low flows (Figure 5). Thus, it is plausible that the hydrodynamic mechanisms which control the main trend of bars migration are similar at low and high discharges. This point is strengthened by that fact that for a bar configuration, the flow structure in the channel does not change significantly with the water discharges (Figures 7, 10, and 11). Therefore, the processes affecting the dynamic of macroforms located in the channel expansion/contraction (described in the next sections) can be applied on an entire hydrological year.

### 5.2.3. Longitudinal Migration of Bars

In the channel, the flow direction is mainly parallel to the left bank in the central and left part of the channel (see arrows Figure 5). The high velocities and bed shear stresses are also located in this part of the channel (Figures 7 and 11). So the bars entering in the system close to the left bank migrate according to this direction until the downstream contraction zone (Figures 5b and 6a). As they are very mobile, these macroforms are named migrating bars. The progradation of the migrating bars is due to the longitudinal migration of the dunes present on their tops and margins [Rodrigues *et al.*, 2012]. More generally, as illustrated by the Figures 5 and 6, the dunes and unit bars govern the morphodynamic of the bars in the studied system, namely their growth, their migration, and their decay (these different steps are detailed in the next sections). This observation is consistent with the study of the dynamic and sedimentary structures of large bars carried out in large sandy braided rivers [Ashworth *et al.*, 2000; Sambrook Smith *et al.*, 2006, 2009].

### 5.2.4. Stop of Downstream Migration of Bars

As see in Figure 5b and observed by Garcia and Nino [1993], Whiting and Dietrich [1993], and Wu *et al.* [2011], with the decrease of the aspect ratio in the downstream contraction zone (Figure 9b), the migration speed of the bars slows down until the bed forms cease their longitudinal migration (along the left bank in the study site). Once the migrating bars have reached the contraction zone, they seem to be forced in this

channel expansion/contraction. Furthermore, as observed in Figures 9a, 12a, and 12b, the flow velocities, the bed shear stresses, and the bed roughnesses (correlated to dunes size, see equation (7)) increase in the contraction zone. This marks a radical change in the bed load transport processes between the expansion area and the contraction zone, and exhibits a transition between the bar and the dune regime. In the narrowing section, the sediments that make up the tail of the bars are then gradually eroded and transported downstream in the form of dunes. So the sediments go out the system but the macroforms stay in it.

This observation demonstrates the influence of the channel width variations (and aspect ratio) on bars' morphodynamics and on the migration velocity of these macroforms.

### 5.2.5. Flow Nonuniformity and Lateral Migration of Bars

When a bar migrates along the left bank, the flow structure is relatively uniform on the cross section, i.e., the hydrodynamic parameters present similar values on each part of the macroform (see P90 and P95 in Figures 7b and 11b).

Simultaneously with the stop of the downstream migration of the bar near the left bank, a unit bar (UB1) appears close to the right bank in the upstream expansion zone (Figure 5b). Then this unit bar grows (probably by the amalgamation of dunes coming from the forced pool FP1) and progrades downstream until merging with the downstream migrating bar in order to form the transverse bar (Figure 6b). This transverse bar is fed by unit bars as UB2 (Figures 5c and 5d) and can be considered as a transverse compound bar [Ashworth *et al.*, 2000, 2011; Sambrook Smith *et al.*, 2006, 2009]. In this configuration, the transverse bar superimposed by large dunes contributes to separate the two currents formed by the channel expansion and therefore forces flows to the left bank and causes a nonuniform distribution of velocities and bed shear stresses within the channel (Figures 7c, 7d, 11c, and 11d). Thus, a cell of high velocities and large bed shear stresses is located on the left side of the bar (or channel), whereas a cell of low velocities and weak bed shear stresses is present on the right side of the macroform (or the channel). The high bed shear stresses increase sediment mobility on the left side of the section and probably promote the sediment transport on the left edge of the bar. Low bed shear stresses limit particle transport on the right side of the section and facilitate the sediment deposition on the right side of the bar (Figure 6c). The nonuniformity of flows over dunes generally causes a heterogeneity of sediment transport along their crests and cause their lateral migration [Dietrich and Smith, 1984; Bridge, 1993; Dalrymple and Rhodes, 1995]. The influence of the flow nonuniformity on the dune direction increases with the bed form's size [Dalrymple, 1984]. Thus, the nonuniform distribution of bed shear stress within the channel encourages the nonuniformity of the transport of the sediments, the lateral migration of the dunes superimposed on the bar and consequently the lateral migration of the macroform from the left bank toward the right bank. In the Jamuna River, a large sandy braided river, Ashworth *et al.* [2000] showed that the development of the flow in an anabranch around a midchannel bar (so the development of the nonuniformity of flow around a midchannel bar) favors its enlargement and then deposition in the anabranch. The deposition deflects the flow across the bar and encourages the elongation of the bar tail. New bars form along the elongated tail of the midchannel bar and make the reach morphology passing from a midchannel pattern to an alternate bar pattern. Despite that the sedimentary processes around the macroforms seem different, our observations and those of Ashworth *et al.* [2000] show that the uniformity or nonuniformity of flow is a key element that determines the evolution and the morphology of bars in a channel.

Then the migrating transverse bar reaches the rip-raps located close to the right bank and ceases its migration since it is not able to migrate downstream and laterally. The bed form becomes a nonmigrating bar. The downstream migration of an upstream macroform increases the deflection of the highest velocities toward the left edge of the nonmigrating bar. This effect combined to the nonuniformity of flows increases the erosion of the left edge of the nonmigrating bed form and the moving of its sediment toward the forced pool close to the right bank (Figure 6e). When the upstream migrating bar reaches the contraction zone, the nonmigrating bar is quasi-totally eroded.

## 6. Conclusions

This field study allows for the first time the observation of the flow structure around bars arranged successively in alternate, lateral, and transversal configurations in a channel expansion/contraction with fixed banks for different water stages.

Primary and secondary velocities, flow directions, bed shear stresses, and bed roughnesses associated to dunes are structured as a function of the morphology and location of the bars. The bars modify the flow structure imposed by the channel width variations. In fact, the macroforms induce a topographic forcing which enables the separation and reducing of the mixing of two currents formed in the upstream channel expansion. Moreover, large dunes migrate mainly on the macroforms. The bed roughness associated to the large dunes increases the turbulences on the bars and also contributes with the topographic forcing to separate the two flows. Since these two currents have different flow characteristics (i.e., different magnitudes of flow velocity, flow direction, bed shear stress, presence or absence of secondary currents), the bars promote the nonuniformity of the flow at the channel's scale.

In turn, the flow structure imposed by the planform and the bars affects the dynamic of dunes and unit bars and consequently the morphodynamic of the bars which migrate in the channel expansion/contraction. The decrease of the channel width and aspect ratio increases the flow velocities and the bed shear stresses. In this hydrodynamic context, the migrating bars become unstable and forced in the channel expansion/contraction. After being forced by the narrowing of the channel, the nonuniformity of the flow causes a nonuniformity of the sediment transport on bars. Thus, the sediments are transported faster on one edge of the macroforms, than on the other edge. This process enables the lateral migration of the bars until they reach a bank and become nonmigrating bars. Finally, the nonmigrating bar stays in the channel expansion/contraction until a new migrating bar enters in the system, deflects the flows and causes its erosion.

For a bar configuration, the flow structure does not change significantly for water discharges varying between low flows and 2 year floods. As the sediments of the sandy-gravel bed river studied are mobile even at low flows, the morphodynamic of the bars in the channel expansion/contraction is continuous during a hydrological year. Nevertheless, it was not possible to determine accurately the upstream boundary conditions and processes involved in the formation or the entrance of bars in the system. Future works implying numerical simulations should be carried out to better understand these mechanisms.

### Notations

$d$	water depth, m.
$D_*$	nondimensional diameter.
$D_{50}$	diameters for which 50% of the particles in weight are finer, m.
$D_{90}$	diameters for which 90% of the particles in weight are finer, m.
$g$	gravitational acceleration ( $9.81 \text{ m s}^{-2}$ ).
$H_D$	mean dune height, m.
$\kappa$	von Karman constant equal to 0.4
$ks$	bed roughness associated to the dunes, m.
$L_D$	mean dune length, m.
$s$	sediment density ratio (2.65).
$u$	horizontal flow velocity $u$ , $\text{m s}^{-1}$ .
$u_E$	easting component of the flow velocities, $\text{m s}^{-1}$ .
$u_N$	northing component of the flow velocities, $\text{m s}^{-1}$ .
$u_P$	primary component of the flow velocities, $\text{m s}^{-1}$ .
$u_S$	secondary component of the flow velocities, $\text{m s}^{-1}$ .
$u_V$	vertical component of the flow velocities, $\text{m s}^{-1}$ .
$W$	channel width, m.
$(z_0)_{SF}$	grain roughness (or the height at which $u = 0$ ), equal to $0.095 D_{90}$ , m.
$\rho$	volumetric mass of water ( $1000 \text{ kg m}^{-3}$ ).
$\rho_s$	volumetric mass of sediment ( $2650 \text{ kg m}^{-3}$ ).
$\tau$	bed shear stress, $\text{N m}^{-2}$ .
$\tau_c$	critical bed shear stress, $\text{N m}^{-2}$ .
$\nu$	kinematic viscosity ( $1 \times 10^{-6} \text{ m}^2 \text{ s}^{-1}$ ).
$\varphi$	orientation of the horizontal flow direction with respect to north, $^\circ$ .
$\psi$	orientation with respect to north of the mean vector velocity on a vertical, $^\circ$ .

## Acknowledgments

This study is part of the PhD thesis of the first author and is funded by the Master Plan Loire Grandeur Nature-FEDER (Presage 30809). The authors thank Benoit Delplancque, Benjamin Gandubert, Olivier Guillemet, and Yann Guerez for their help during the measurements. The authors thank the Associate Editor and the two anonymous reviewers for their comments that led to significantly improve the manuscript.

## References

- Ashmore, P. E. (1982), Laboratory modelling of gravel braided stream morphology, *Earth Surf. Processes Landforms*, *7*, 201–225.
- Ashmore, P. E. (1991), How do gravel-bed rivers braid, *Can. J. Earth Sci.*, *28*, 326–341.
- Ashworth, P. J. (1996), Mid-channel bar growth and its relationship to local flow strength and direction, *Earth Surf. Processes Landforms*, *21*, 103–123.
- Ashworth, P. J., R. I. Ferguson, P. E. Ashmore, C. Paola, D. M. Powell, and K. L. Prestegards (1992), Measurements in a Braided River chute and lobe: 2. Sorting of bed load during entrainment, transport, and deposition, *Water Resour. Res.*, *28*, 1887–1896.
- Ashworth, P. J., J. L. Best, J. E. Roden, C. S. Bristow, and G. J. Klaassen (2000), Morphological evolution and dynamics of a large, sand braided bar, Jamuna River, Bangladesh, *Sedimentology*, *47*, 533–555, doi:10.1046/j.1365-3091.2000.00305.x.
- Ashworth, P. J., G. H. S. Smith, J. L. Best, J. S. Bridge, S. N. Lane, I. A. Lunt, A. J. H. Reesink, C. J. Simpson, and R. E. Thomas (2011), Evolution and sedimentology of a channel fill in the sandy braided South Saskatchewan River and its comparison to the deposits of an adjacent compound bar, *Sedimentology*, *58*, 1860–1883, doi:10.1111/j.1365-3091.2011.01242.x.
- Belleudy, P. (2000), Restoring flow capacity in the Loire River bed, *Hydrol. Processes*, *14*, 2331–2344, doi:10.1002/1099-1085(200009)14:13.
- Bernini, A., V. Caleffi, and A. Valiani (2006), Numerical modelling of alternate bars, in *Braided Rivers: Process, Deposits, Ecology and Management*, *Spec. Publ.*, *36*, edited by G. H. S. Smith et al., pp. 153–175, Blackwell, Oxford, U. K.
- Best, J. L. (1987), Flow dynamics at river channel confluences: Implications for sediment transport and bed morphology, in *Recent Developments in Fluvial Sedimentology*, *SEPM Spec. Publ.*, *39*, edited by F. G. Ethridge et al., pp. 27–35, Spec. Publ. Soc. Econ. Paleontol. Miner., Tulsa, Okla.
- Biron, P. M., and S. N. Lane (2008), Modelling hydraulics and sediment transport at river confluences, in *River Conferences, Tributaries and the Fluvial Network*, edited by S. P. Rice et al., pp. 17–44, John Wiley, Chichester, U. K.
- Bittner, L. D. (1994), River bed response to channel width variations: Theory and experiments, MS thesis, Univ. of Ill., Urbana-Champaign.
- Blondeaux, P., and G. Seminara (1985), A unified bar-bend theory of river meanders, *J. Fluid Mech.*, *157*, 449–470.
- Bravard, J. P., et al. (1997), River incision in south east France: Morphological phenomena and ecological effects, *Reg. Rivers Res. Manage.*, *13*, 75–90.
- Bridge, J. S. (1993), The interaction between channel geometry, water flow, sediment transport and deposition in braided rivers, in *Braided Rivers*, edited by J. L. Best and C. S. Bristow, pp. 13–71, Geological Society Special Publication, London, U. K.
- Bridge, J. S. (2003), *Rivers and Floodplains: Forms, Processes, and Sedimentary Record*, 491 pp., Blackwell, Oxford, U. K.
- Bridge, J. S., and S. L. Gabel (1992), Flow and sediment dynamics in a low sinuosity, braided river: Calamus River, Nebraska Sandhills, *Sedimentology*, *39*, 125–142.
- Bridge, J. S., and J. Jarvis (1982), The dynamics of a river bend: A study in flow and sedimentary processes, *Sedimentology*, *29*, 499–541.
- Callander, R. A. (1969), Instability and river channels, *J. Fluid Mech.*, *36*, 465–480.
- Claude, N. (2012), Processus et flux hydro-sédimentaires en rivière sablo-graveleuse: Influence de la largeur de section et des bifurcations en Loire moyenne (France), PhD thesis, 366 pp., Univ. de Tours, Tours, France.
- Claude, N., S. Rodrigues, V. Bustillo, J.-G. Bréhéret, J.-J. Macaire, and P. Jugé (2012), Estimating bedload transport in a large sand-gravel bed river from direct sampling, dune tracking and empirical formulae, *Geomorphology*, *179*, 40–57, doi:10.1016/j.geomorph.2012.07.030.
- Colombini, M., G. Seminara, and M. Tubino (1987), Finite-amplitude alternate bars, *J. Fluid Mech.*, *181*, 213–232.
- Cornell, C. A. (1972), First order analysis of model and parameter uncertainty, in *International Symposium on Uncertainties in Hydrology and Water Resources Systems*, vol. 3, pp. 1245–1272, Univ. of Ariz., Tucson.
- Crosato, A., and E. Mosselman (2009), Simple physics-based predictor for the number of river bars and the transition between meandering and braiding, *Water Resour. Res.*, *45*, W03424, doi:10.1029/2008WR007242.
- Crosato, A., E. Mosselman, F. Beidmarim Desta, and W. S. J. Uijtewaal (2011), Experimental and numerical evidence for intrinsic nonmigrating bars in alluvial channels, *Water Resour. Res.*, *47*, W03511, doi:10.1029/2010WR009714.
- Crosato, A., F. B. Desta, J. Cornelisse, F. Schuurman, and W. S. J. Uijtewaal (2012), Experimental and numerical findings on the long-term evolution of migrating alternate bars in alluvial channels, *Water Resour. Res.*, *48*, W06524, doi:10.1029/2011WR011320.
- Dalrymple, R. W. (1984), Morphology and internal structure of sandwaves in the Bay of Fundy, *Sedimentology*, *31*, 365–382.
- Dalrymple, R. W., and R. N. Rhodes (1995), Estuarine dunes and bars, in *Geomorphology and Sedimentology of Estuaries*, *Dev. Sedimentol.*, *53*, edited by G. M. E. Perillo, pp. 359–422, Elsevier, Amsterdam, The Netherlands.
- De Serres, B., A. G. Roy, P. M. Biron, and J. L. Best (1999), Three-dimensional structure of flow at a confluence of river channels with discordant beds, *Geomorphology*, *26*, 313–335.
- Defina, A. (2003), Numerical experiments on bar growth, *Water Resour. Res.*, *39*(4), 1092, doi:10.1029/2002WR001455.
- Détriché, S., S. Rodrigues, J.-J. Macaire, P. Bonté, J.-G. Bréhéret, J.-P. Bakyono, and P. Jugé (2010), Caesium-137 in sandy sediments of the River Loire (France): Assessment of an alluvial island evolving over the last 50 years, *Geomorphology*, *115*, 11–22, doi:10.1016/j.geomorph.2009.07.003.
- Dietrich, W. E., and J. D. Smith (1983), Influence of the point bar on flow through curved channels, *Water Resour. Res.*, *19*, 1173–1192.
- Dietrich, W. E., and J. D. Smith (1984), Bed load transport in a river meander, *Water Resour. Res.*, *20*, 1355–1380.
- Dinehart, R. L., and J. R. Burau (2005a), Averaged indicators of secondary flow in repeated acoustic Doppler current profiler crossings of bends, *Water Resour. Res.*, *41*, W09405, doi:10.1029/2005WR004050.
- Dinehart, R. L., and J. R. Burau (2005b), Repeated surveys by acoustic Doppler current profiler for flow and sediment dynamics in a tidal river, *J. Hydrol.*, *314*, 1–21, doi:10.1016/j.jhydrol.2005.03.019.
- Federici, B., and C. Paola (2003), Dynamics of channel bifurcations in noncohesive sediments, *Water Resour. Res.*, *39*(6), 1162, doi:10.1029/2002WR001434.
- Ferguson, R. I., P. E. Ashmore, P. J. Ashworth, C. Paola, and K. L. Prestegard (1992), Measurements in a braided river chute and lobe 1. Flow pattern, sediment transport, and channel change, *Water Resour. Res.*, *28*, 1877–1886.
- Fredsoe, J. (1978), Meandering and braiding of rivers, *J. Fluid Mech.*, *84*, 609–624.
- Garcia, M., and Y. Nino (1993), Dynamics of sediment bars in straight and meandering channels: Experiments on the resonance phenomenon, *J. Hydraul. Res.*, *31*, 739–761.
- Ikeda, S., and G. Parker (1989), *River Meandering*, *Water Resour. Monogr.*, *12*, 489 pp., AGU, Washington, D. C.
- Jackson, R. G. (1975), Hierarchical attributes and a unifying model of bed forms composed of cohesionless material and produced by shearing flow, *Bull. Geol. Soc. Am.*, *86*, 1523–1533.
- Julien, P. Y., G. J. Klaassen, W. B. M. Ten Brinke, and A. W. E. Wilbers (2002), Case study: Bed resistance of Rhine River during 1998 flood, *J. Hydraul. Eng.*, *128*, 1042–1050.

- Kasvi, E., M. Vaaja, P. Alho, H. Hannu, J. Hyypää, H. Kaartinen, and A. Kukko (2013), Morphological changes on meander point bars associated with flow structure at different discharges, *Earth Surf. Processes Landforms*, **38**, 577–590, doi:10.1002/esp.3303.
- Kiss, T., and G. Sipos (2007), Braid-scale channel geometry changes in a sand-bedded river: Significance of low stages, *Geomorphology*, **84**, 209–221, doi:10.1016/j.geomorph.2006.01.041.
- Kleinhans, M. G., and J. H. van den Berg (2011), River channel and bar patterns explained and predicted by an empirical and a physics-based method, *Earth Surf. Processes Landforms*, **36**, 721–738, doi:10.1002/esp.2090.
- Lane, S. N., K. F. Bradbrook, K. S. Richards, P. M. Biron, and A. G. Roy (2000), Secondary circulation cells in river channel confluences: Measurement artefacts or coherent flow structures?, *Hydrol. Processes*, **14**, 2047–2071, doi:10.1002/1099-1085.
- Lanzoni, S. (2000a), Experiments on bar formation in a straight flume: 1. Uniform sediment, *Water Resour. Res.*, **36**, 3337–3349, doi: 10.1029/2000WR900160.
- Lanzoni, S. (2000b), Experiments on bar formation in a straight flume: 2. Graded sediment, *Water Resour. Res.*, **36**, 3351–3363, doi: 10.1029/2000WR900161.
- Leopold, L. B., and M. G. Wolman (1957), River channel patterns: Braided, meandering, and straight, *U.S. Geophys. Surv., Prof. Pap.*, **262-B**, 39–85.
- Lewin, J. (1976), Initiation of bed forms and meanders in coarse-grained sediment, *Bull. Geol. Soc. Am.*, **87**, 281–285.
- Lisle, T. E., H. Ikeda, and F. Iseya (1991), Formation of stationary alternate bars in a steep channel with mixed-size sediment: A flume experiment, *Earth Surface Processes and Landforms*, **16**, 463–469.
- Luchi, R., J. M. Hooke, G. Zolezzi, and W. Bertoldi (2010a), Width variations and mid-channel bar inception in meanders: River Bollin (UK), *Geomorphology*, **119**, 1–8, doi:10.1016/j.geomorph.2010.01.010.
- Luchi, R., G. Zolezzi, and M. Tubino (2010b), Modelling mid-channel bars in meandering channels, *Earth Surf. Processes Landforms*, **35**, 902–917, doi:10.1002/esp.1947.
- McLelland, S. J., P. J. Ashworth, and J. L. Best (1994), Velocity correction methods in open channels: Description, critique and recommendations, *Consult. Rep. FAP24*, Dhaka, Bangladesh.
- McLelland, S. J., P. J. Ashworth, J. L. Best, J. Roden, and G. J. Klaassen (1999), Flow structure and transport of sand-grade suspended sediment around an evolving braid bar, Jamuna River, Bangladesh, in *Fluvial Sedimentology VI: International Association of Sedimentologists, Spec. Publ. 28*, edited by N. D. Smith and J. Rogers, pp. 43–57, Blackwell, Oxford, U. K.
- Nicholas, A. P., and G. H. S. Smith (1999), Numerical simulation of three-dimensional flow hydraulics in a braided channel, *Hydrol. Processes*, **13**, 913–929.
- Paarlberg, A. J., C. M. Dohmen-Janssen, S. J. M. H. Hulscher, P. Termes, and R. Schielen (2010), Modelling the effect of time-dependent river dune evolution on bed roughness and stage, *Earth Surf. Processes Landforms*, **35**, 1854–1866, doi:10.1002/esp.2074.
- Parker, G. (1976), On the cause and characteristic scales of meandering and braiding in rivers, *J. Fluid Mech.*, **76**, 457–480.
- Parsons, D. R., J. L. Best, S. N. Lane, O. Orfeo, R. J. Hardy, and R. Kostaschuk (2007), Form roughness and the absence of secondary flow in a large confluence-diffuence, Rio Parana, Argentina, *Earth Surf. Processes Landforms*, **32**, 155–162, doi:10.1002/esp.1457.
- Rennie, C. D., and M. Church (2010), Mapping spatial distributions and uncertainty of water and sediment flux in a large gravel bed river reach using an acoustic Doppler current profiler, *J. Geophys. Res.*, **115**, F03035, doi:10.1029/2009JF001556.
- Repetto, R., M. Tubino, and C. Paola (2002), Planimetric instability of channels with variable width, *J. Fluid Mech.*, **457**, 79–109, doi:10.1017/S0022112001007595.
- Rhoads, B. L., and S. T. Kenworthy (1995), Flow structure at an asymmetrical stream confluence, *Geomorphology*, **11**, 273–293.
- Richardson, W. R., and C. R. Thorne (1998), Secondary currents around braid bar in Brahmaputra River, Bangladesh, *J. Hydraul. Eng.*, **124**, 325–327.
- Richardson, W. R., and C. R. Thorne (2001), Multiple thread flow and channel bifurcation in a braided river: Brahmaputra-Jamuna River, Bangladesh, *Geomorphology*, **38**, 185–196, doi:10.1016/S0169-555X(00)00080-5.
- Richardson, W. R., C. R. Thorne, and S. Mahmood (1996), Secondary flow and channel changes around a bar in the Brahmaputra river, Bangladesh in *Coherent Flow Structures in Open Channels*, edited by P. J. Ashworth et al., pp. 519–543, John Wiley, Chichester, U. K.
- Rodrigues, S., and N. Claude (2010), Le transport solide de la Loire: Des sédiments sans cesse en mouvement, *Géosciences*, **12**, 110.
- Rodrigues, S., J. G. Bréhéret, J. J. Macaire, F. Moatar, D. Nistoran, and P. Jugé (2006), Flow and sediment dynamics in the vegetated secondary channels of an anabranching river: The Loire River (France), *Sediment. Geol.*, **186**, 89–109, doi:10.1016/j.sedgeo.2005.11.011.
- Rodrigues, S., J.-G. Bréhéret, J. J. Macaire, S. Greulich, and M. Villar (2007), In channel woody vegetation controls on sedimentary processes and the sedimentary record within alluvial environments: A modern example of an anabranch of the River Loire, France, *Sedimentology*, **54**, 223–242, doi:10.1111/j.1365-3091.2006.00832.x.
- Rodrigues, S., N. Claude, P. Juge, and J. G. Breheret (2012), An opportunity to connect the morphodynamics of alternate bars with their sedimentary products, *Earth Surf. Processes Landforms*, **37**, 240–248, doi:10.1002/esp.2255.
- Rozovskii, I. (1954), Concerning the question of velocity distribution in stream bends, DAN URSR (Report of the Academy of Sciences of the Ukraine SSR), Kiev, Ukraine.
- Seminara, G., and M. Tubino (1989), Alternate bars and meandering: Free, forced and mixed interactions, in *River Meandering, Water Resour. Monogr. 12*, edited by S. Ikeda and G. Parker, pp. 267–320, AGU, Washington, D. C.
- Smith, G. H. S., P. J. Ashworth, J. L. Best, J. Woodward, and C. J. Simpson (2006), The sedimentology and alluvial architecture of the sandy braided South Saskatchewan River, Canada, *Sedimentology*, **53**, 413–434, doi:10.1111/j.1365-3091.2005.00769.x.
- Smith, G. H. S., P. J. Ashworth, J. L. Best, I. A. Lunt, O. Orfeo, and D. R. Parsons (2009), The sedimentology and alluvial architecture of a large braid bar, Rio Parana, Argentina, *J. Sediment. Res.*, **79**, 629–642, doi:10.2110/jsr.2009.066.
- Sime, L. C., R. I. Ferguson, and M. Church (2007), Estimating shear stress from moving boat acoustic Doppler velocity measurements in a large gravel bed river, *Water Resour. Res.*, **43**, W03418, doi:10.1029/2006WR005069.
- Smith, N. D. (1978), Some comments on terminology for bars in shallow rivers, in *Fluvial Sedimentology*, edited by A. D. Miall, pp. 85–88, Can. Soc. Petrol. Geol. Mem. Calgary, Canada.
- Struikma, N., K. W. Olesen, C. Flokstra, and H. J. De Vriend (1985), Bed deformation in curved alluvial channels, *J. Hydraul. Res.*, **23**, 57–79.
- Szupiany, R. N., M. L. Amsler, J. L. Best, and D. R. Parsons (2007), Comparison of fixed- and moving-vessel flow measurements with an aDp in a large river, *J. Hydraul. Eng.*, **133**, 1299–1308, doi:10.1061/(ASCE)0733-9429(2007)133:12(1299).
- Szupiany, R. N., M. L. Amsler, D. R. Parsons, and J. L. Best (2009), Morphology, flow structure, and suspended bed sediment transport at two large braid-bar confluences, *Water Resour. Res.*, **45**, W05415, doi:10.1029/2008WR007428.
- Szupiany, R. N., M. L. Amsler, J. Hernandez, D. R. Parsons, J. L. Best, E. Fornari, and A. Trento (2012), Flow fields, bed shear stresses, and suspended bed sediment dynamics in bifurcations of a large river, *Water Resour. Res.*, **48**, W11515, doi:10.1029/2011WR011677.
- Tubino, M. (1991), Growth of alternate bars in unsteady flow, *Water Resour. Res.*, **27**, 37–52.

- Van der Mark, C. F., A. Blom, and S. J. M. H. Hulscher (2008), Quantification of variability in bedform geometry, *J. Geophys. Res.*, *113*, F03020, doi:10.1029/2007JF000940.
- Van Rijn, L. C. (1984), Sediment transport, part III: Bed forms and alluvial roughness, *J. Hydraul. Eng.*, *110*, 1733–1754.
- Whiting, P. J., and W. E. Dietrich (1991), Convective accelerations and boundary shear stress over a channel bar, *Water Resour. Res.*, *27*, 783–796.
- Whiting, P. J., and W. E. Dietrich (1993), Experimental constraints on bar migration through bends: Implications for meander wavelength selection, *Water Resour. Res.*, *29*, 1091–1102.
- Wilcock, P. R. (1996), Estimating local bed shear stress from velocity observations, *Water Resour. Res.*, *32*, 3361–3366.
- Wright, S. A., and M. Kaplinski (2011), Flow structures and sandbar dynamics in a canyon river during a controlled flood, Colorado River, Arizona, *J. Geophys. Res.*, *116*, F01019, doi:10.1029/2009JF001442.
- Wu, F. C., and T. H. Yeh (2005), Forced bars induced by variations of channel width: Implications for incipient bifurcation, *J. Geophys. Res.*, *110*, F02009, doi:10.1029/2004JF000160.
- Wu, F. C., Y. C. Shao, and Y. C. Chen (2011), Quantifying the forcing effect of channel width variations on free bars: Morphodynamic modeling based on characteristic dissipative Galerkin scheme, *J. Geophys. Res.*, *116*, F03023, doi:10.1029/2010JF001941.
- Yalin, M. S., and M. Selim (1992), *River Mechanics*, Pergamon, Oxford, U. K.